Impact of Inhibition Delays on Theta Rhythms in Hippocampal Microcircuits: A Computational Modelling Approach

Parineeta Ekhande
Student Number: 14295083
Supervisor: Dr. Fleur Zeldenrust

Research Project 2
Masters in Brain and Cognitive Sciences

Abstract:
The hippocampus plays a critical role in cognitive processes such as memory encoding, driven by the precise timing of inhibitory and excitatory signals within its neuronal circuits. Disruptions in these signals, particularly due to demyelination, can lead to alterations in the rhythmic oscillations essential for proper brain function. This thesis investigates the impact of synaptic delays on theta rhythm modulation within a hippocampal microcircuit comprising of pyramidal cells and fast-spiking interneurons. Using computational modelling, a feedforward circuit of one two-compartment Pinsky-Rinzel model for pyramidal neurons and one Wang-Buzsáki model for interneuron was made. The circuit simulates the effects of varying synaptic conductance and delays on the changes in activity of the pyramidal cell.

The model reveals that even minor delays in inhibitory signal can disrupt the synchrony required for excitatory and inhibitory balance of activity. By analysing the firing rates, inter-spike intervals, activity patterns pyramidal cells under different synaptic delay conditions, power spectrums and correlations, this project demonstrates how demyelination-induced delays in inhibitory input may lead to the slowing or disruption of theta rhythms. The findings highlight the critical role of maintaining proper network dynamics, providing a possible explanation for underlying disruption of theta rhythm due to demyelinated interneurons.

1. Introduction

The brain is a complex dynamical system made up of billions of interconnected neurons. Information is processed and transmitted through the network of neurons in the form of action potentials. The transmission and processing are achieved through precisely timed inhibition and activation of neurons. The neurons respond to action potentials generated by other neurons that are oscillatory by nature. The temporal dynamics of this signal plays a crucial role in information processing and cognitive processes such as memory encoding (Stella & Reeves, 2011). The oscillations provide the code for brain's internal communication and their modulation becomes key to understand brain function. Disruption in these oscillations brought on by neurogenerative diseases directly affects the electrical transmissions in local brain circuits (Dubey et al. 2022). One physical manifestation of this is the shedding of the protective layer around neurons called myelin sheath. The shedding – known as demyelination causes Multiple Sclerosis. The loss of myelin in neurons slows down their ability to transmit electrical signals - directly destabilising local neuronal networks leading to alterations the brain rhythms.

Local neural circuits in any specific region in the brain contain inhibitory and excitatory neurons. For instance, in the hippocampus, there are Pyramidal cells - the primary excitatory neurons (hereon referred to as PC), and various inhibitory interneurons, such as basket cells, parvalbumin-positive (PV+) and O-LM cells which work together to regulate the flow of information through action potentials (Dubey et al. 2022). Interneurons send precisely timed inhibitory signals to the PC as they are strongly and reciprocally connected to each other (Bartos et al. 2002; Gonchar & Burkhalter, 1997; Tamás et al. 1997). Furthermore, diverse groups of interneurons provide different forms of inhibition that affect the excitatory activity of pyramidal cells, which are sensitive to this inhibitory input and perform computations accordingly (Klausberger, 2009; Zeldenrust & Wadman, 2012).

Studies have shown two distinct forms of inhibition in the CA3 area of the hippocampus - O-LM interneurons connected to dendrites of PCs and basket type interneurons connected to the soma (Gloveli et al. 2005; Gloveli et al. 2005). This delicate balance between inhibition and excitation drives theta and gamma rhythms in the hippocampus (Zeldenrust & Wadman, 2009). Any disruption in this balance can subsequently alter these rhythms. A form of disruption can be through demyelination of interneurons. A recent study by Dubey et al. (2022) showed that demyelination of PV+ interneurons lead to delays in inhibition of PCs causing precession of theta oscillations. Thus, we aimed to explore the question – can an increase in delay of inhibition, between the PC and interneuron lead to subsequent slowing down of the theta rhythm.

Computational studies involving modelling of interneuron – PC microcircuit show two distinct loops in which they are connected, and these loops operate at different kinetics affecting hippocampal functions including the generation, transfer and phase precession of theta, gamma and delta rhythms (Booth & Bose, 2001a; Bose et al. 2000; Kamondi et al. 1998; Tiesinga et al. 2001; Tort et al. 2007; Whittington et al. 2000). Simulations studying the dynamics of PC and interneuron interactions show their significance in generating rate and temporal codes within these circuits (Booth & Bose, 2001a; 2001b; Booth et al. 2000; Booth & Bose, 2002) The interneuron connected to the dendrite of PC can synchronize the burst activity of PC.

Slow-decaying inhibition plays a vital role in this synchronization even without a direct excitatory connection between them (Booth & Bose, 2001a; 2001b). The insights from Booth & Bose (2001a; 2001b) suggest that the delay in inhibition reaching the soma, due to the separation of soma and dendrite, aids this synchronization. Additionally, inhibition from the interneuron modulates the firing mode of the PC. An increase in the maximal conductance of inhibitory input transitions the firing from complex bursts to bursts with multiple spikes, and eventually to single spikes, thus significantly influencing the firing patterns of pyramidal cells. This modulation of firing patterns suggests that the precise timing of inhibition is crucial for maintaining rhythmic oscillations and increase in the delay of this inhibition could result in a disturbance of theta rhythm reflecting dynamic interplay between excitation and inhibition in neural circuits.

So far, there are two ways in which the circuits have been modelled - feedback loop models and feed-forward loop models (Bose et al. 2000; Booth & Bose, 2001a; 2001b; Zeldenrust & Wadman, 2009; 2012). Feedback inhibition is a neutral circuit wherein the excitatory neuron inhibits or stabilizes itself through its own output (Jonas & Buzsaki, 2007; Mittmann et al. 2004), or to produce oscillations between the excitatory and inhibitory cells (Wilson & Cowan, 1973). Zeldenrust & Wadman (2009) found that feedback inhibition affects the firing mode (bursts or spikes) of the excitatory cell. An inhibitory postsynaptic current (IPSC) generated by a feedback loop responds to the activity of the PC, whereas IPSCs from feed-forward inhibition can occur independent of the PC activity. This enhances the potential for varied spike timing between PCs and interneurons. Consequently, feed-forward inhibition can offer more variability in output than feedback inhibition. In feedforward inhibition, the interneuron and PC both receive a common input. The simultaneous activation results in a stronger initial response followed by a weaker response at the end (Zeldenrust & Wadman, 2012). This enhances the precision of firing by narrowing the temporal window, allowing PC to fire spikes at full strength only before the interneuron activates (Jonas & Buzsaki, 2007; Mittmann et al. 2004; Pouille & Scanziani, 2001). The dynamics of synaptic connections, particularly the rise and decay time constants of inhibitory input from interneurons, are crucial in shaping the firing behavior of PCs; altering these parameters modifies the bursting behavior, indicating the network's sensitivity to change (Booth & Bose, 2001b). The study by Booth & Bose, 2002 show that inhibition arriving at different times during the burst cycle can significantly affect the firing dynamics. For instance, inhibition arriving during a burst can change the firing patterns of the PCs. Slow dendritic inhibition and fast somatic inhibition have different effects on the properties of PCs (Zeldenrust & Wadman, 2012). The timing and strength of inhibitory inputs can lead to different firing modes, such as bursts or a single spike.

The presence of synaptic delays and the timing of synaptic excitation and inhibition can lead to synchronized bursting patterns in the network, which is crucial for normal cortical activity. Thus, to understand the interactions of the local circuits in a brain with neurodegenerative disease such as MS, we can use such computational studies to understand the inherent activity of the abnormal neurons. The CA3 region of the hippocampus generates synchronized epileptiform bursts under a variety of experimental situations in which inhibition has been reduced (Pinsky & Rinzel, 1994).

As validated by Dubey et al. (2022), demyelination of interneurons leads to an increase in theta power in mice brains. It also causes decrease in PV+ interneuron's inhibitory activity but does not affect excitatory drive of PV+BC interneurons. Thus, the goal of the present study was to investigate the potential relationship between synaptic conductance and increase in the delay of inhibition as a way to simulate demyelination of interneurons.

To this avail, we create a microcircuit model of a single cell two-compartment PC modelled using Pinsky and Rinzel neuron model and a single compartment interneuron modelled using Wang and Buszaki interneuron model. In the circuit, the interneuron and the soma and dendrite of the PC are connected via an inhibitory synapse and for making the circuit feedforward, external current is given both to the interneuron and the PC. The model simulates varying degrees of synaptic delays to assess the effects of theta rhythm modulation, to reveal whether minor alternations in inhibition timing can disrupt the delicate synchrony necessary for theta oscillations to persist effectively in the network dynamics. The circuit is stimulated using the Frozen Noise Protocol developed by Zeldenrust et al. (2017), a detailed explanation is given in the following sections.

2. Microcircuit Model

To create tractable model of the hippocampal microcircuit of PC and interneuron, we modelled the basic circuit of primary excitatory neuron i.e. the PC using the Pinsky & Rinzel (1994) model and inhibitory interneuron using fast spiking Wang & Buszaki (1996) interneuron model.

The model is simulated in Brian Simulator. All the simulations were run for a total of 180 seconds (3 minutes). The basic circuits consist of one PC and one interneuron cell connected either to the soma or dendrite compartment of the PC. The inhibition is dependent on the location of connection the inhibitory synapse with an exponential rise and decay. The coneection of the interneuron to the soma is with fast kinetics (τ rise = 1ms; τ decay = 5ms – termed fast somatic inhibtion), The connection of interneuron to dendrite is with slow kinectics (τ rise = 5ms ; τ decay = 20ms – slow dendritic inhibition) Banks et al. (1998); Banks et al. (2000); Miles et al. (1996); Pearce (1993); White et al. (2000)). The synaptic conductances were varied at three levels : 2mS, 4mS, 8mS and the synaptic delays ranging from 0ms to 5ms in steps of 0.5ms were introduced.

The Pinsky & Rinzel (1994) is a reduction of a more complicated CA3 neuron model developed by Traub et al. (1991). It is a two-compartment model capturing the distinction between firing characteristics of a soma and dendrite. The somatic compartment consists of a sodium current, delayed-rectifier potassium current and a leak current. The dendritic compartment consists of calcium-activated ionic currents - calcium current, calcium-activated potassium current, calcium and potassium dependent, after hyperpolarisation calcium-induced potassium current and leak current. The two compartments are equal in size, and electrically connected and cell as a whole can generate both spikes and bursts depending on the injected current and conductance (Fig .2.)

The interneuron is a single-compartment fast-spiking neuron model developed by Wang & Buszaki (1996). It has a sodium current, a potassium current and a leak current. It has an input-output curve for constant inputs (Zeldenrust & Wadman, 2009), fires at high frequencies making it a good model for modelling fast-spiking interneurons.

All the synapses are activated by a presynaptic spike or burst. Their opening and closing are modelled using 'Synapse' equations given in the appendix.

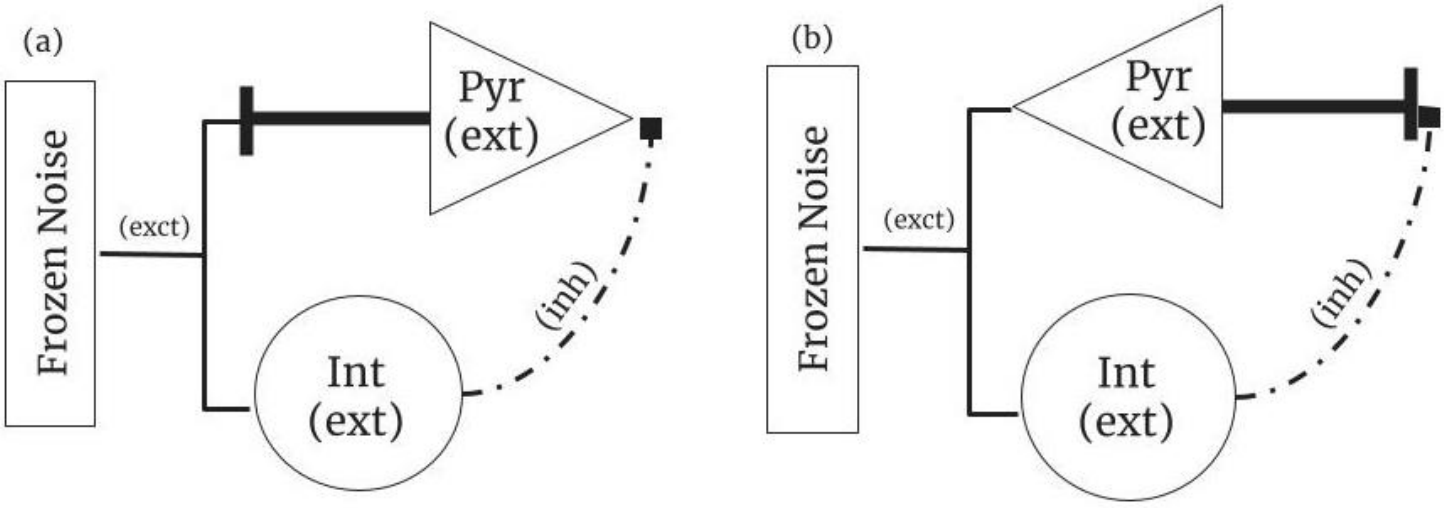

Fig. 1. Schematic of the microcircuit model. (a) is somatic inhibition and (b) is dendritic inhibition

2.1.2. Input Current:

The input used for the model is the Frozen noise protocol developed by Zeldenrust et al. (2017). The process as explained by Zeldenrust et al. (2017), the input generation begins with the assumption that neurons respond to the presence or absence of a preferred stimulus feature, represented by a hidden state *x*. This hidden state is a binary variable where $x = 1$ indicates the presence of the stimulus, and $x = 0$ indicates its absence. The appearance and disappearance of this stimulus follow a Markov process characterized by rates r_{on} and r_{off}. The neuron does not directly observe the hidden state. Instead, they receive synaptic inputs from a population of *N* presynaptic neurons, each firing a Poisson spike trains at rates $q_{i,on}$ when $x = 1$, and $q_{i,off}$ when $x = 0$.

The total synaptic input to the neuron is calculated as

$$I = \sum_{i=I}^{N} w_i s_i * k(t) \quad (1)$$

where s_i is the spike train of presynaptic neuron *i*, and *k(t)* is the exponential kernel. This input current cannot be directly used in experiments or models without scaling it from dimensionless units to amperes (A). w_i are the weights. The synaptic weights are defined by

$$w_i = \log \frac{q_{on}^i}{q_{off}^i} \quad (2)$$

The weights are positive or negative depending on the firing rate of the presynaptic neuron. If the rate in the 'on' state of the hidden state is higher than rate in the 'off' state ($q_{on}^{i} > q_{off}^{i}$), the weights are positive ($w_i > 0$) and vice versa.

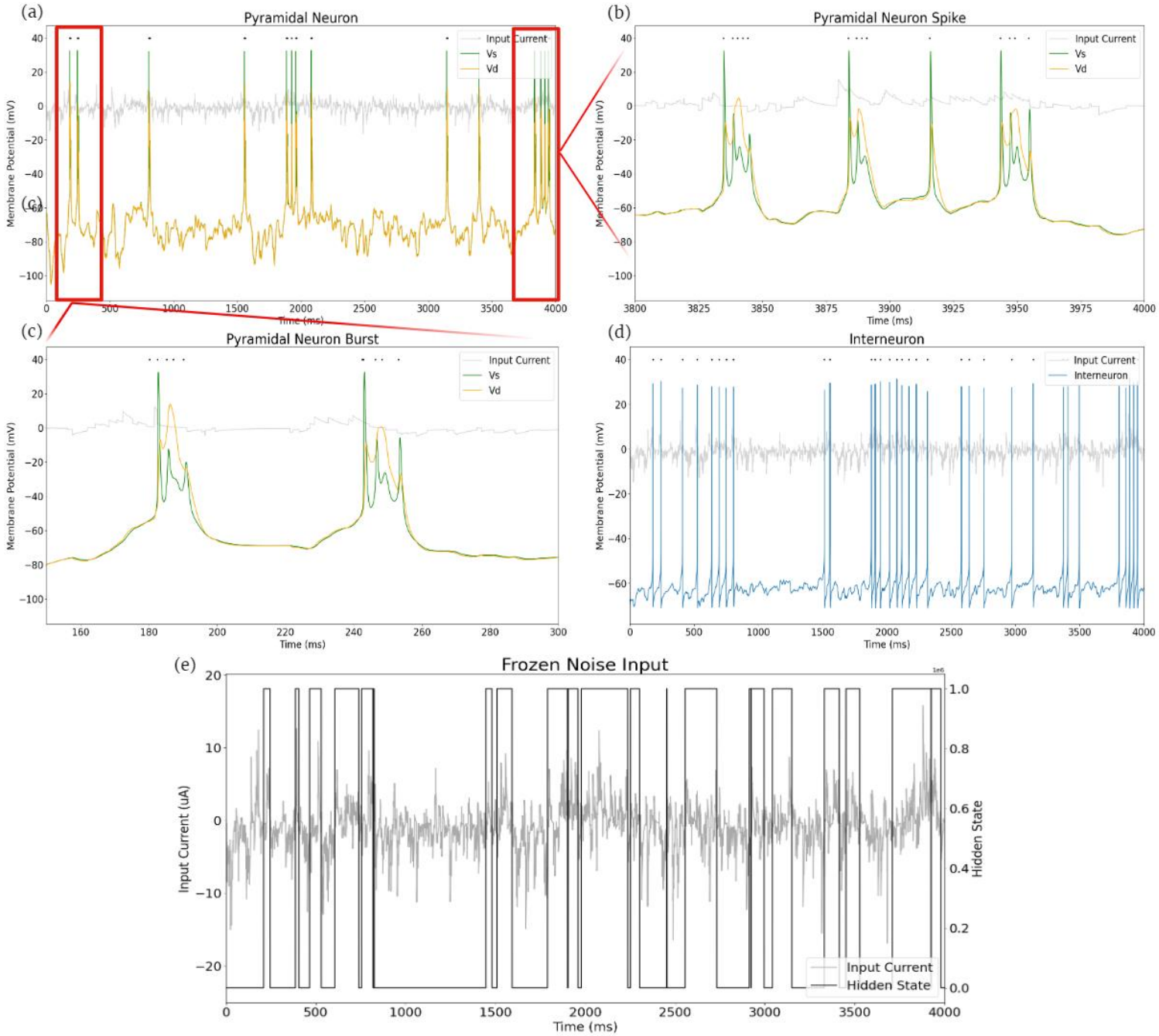

Fig. 2. Activity of pyramidal cell and interneuron in response to frozen noise protocol at 20khz sampling rate. (a) Pyramidal cell activity (both burst and spike) in control condition of no synaptic conductance and delay (gsyn=0mS; delay=0ms). (b) Pyramidal cell burst (c) Pyramidal cell spike (d) Interneuron spikes (e) representation of frozen noise input current with hidden states

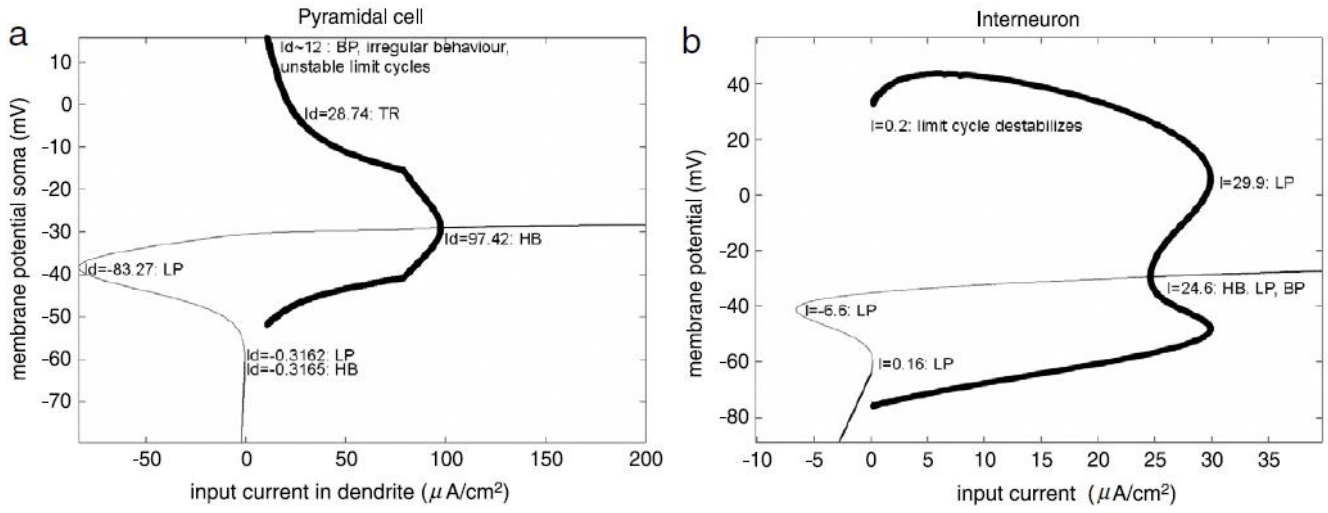

Fig. 3. Bifurcation diagrams were created for two neuron models, the Pinsky and Rinzel (1994) pyramidal cell model and the Wang and Buzsáki (1996) interneuron model by Zeldenrust & Wadman, 2009 using Bard Ermentrout's XPPAUT software. For the pyramidal cell, when a negative current is injected into the dendrite (Id < -0.3 mA/cm²), the cell remains inactive. As the injected current increases, the cell begins to spike. At low current levels, it shows slow bursting activity. As the current increases further, the cell transitions from bursting to irregular spiking, and then to regular spiking with decreasing spike amplitude. The spiking activity stops through a Hopf bifurcation when Id reaches about 97 mA/cm².
The interneuron stays inactive with negative and very small positive currents. It starts spiking when the current reaches about 0.2 mA/cm². Between 24.6 mA/cm² and 30 mA/cm², the neuron can either spike with low amplitude or stay inactive, indicating a bistable state. For currents higher than 30 mA/cm², the neuron becomes inactive again. The diagrams use thin lines for unstable fixed points, thick lines for stable fixed points, and very thick lines for (un)stable limit cycles, indicating the minimum and maximum values. (Zeldenrust & Wadman, 2009)
LP (limit point), HB (Hopf bifurcation), TR (torus bifurcation), and BP (branching point).

(Reprinted from Two forms of feedback inhibition determine the dynamical state of a small hippocampal network (Zeldenrust & Wadman, 2009), Copyright 2009 by Elsevier Inc. Reprinted with permission.)

2.1.2. Input Parameters:

Since PCs are primary excitatory neurons, they show regular spiking activity whereas the interneurons are fast spiking neuron to provide fast inhibition to the PC. This does not allow for the same input current parameters to be given for both the cells. The time constant of the hidden state (Tau) is set at 50ms with sampling frequency of 20kHz (timestep (dt) = 0.05ms). The scaling parameter of the input current for the PC is set to be at 20 with an amplitude (baseline) of -0.4. For the interneuron, the scaling parameter is set at 2 with and amplitude of 0.2 (parameters are initially set to be dimensionless however in the equation for setting the injected current, its converted to amperes (A) for current clamp setting).

Thus, the frozen noise input current is generated with the following equation:

$$Input_{injected} = I_{scale} * I_{theory} + I_{baseline}$$

Wherein, I_{scale} is the scaling parameter, I_{theory} is the input data and $I_{baseline}$ is the amplitude to scale the injected input.

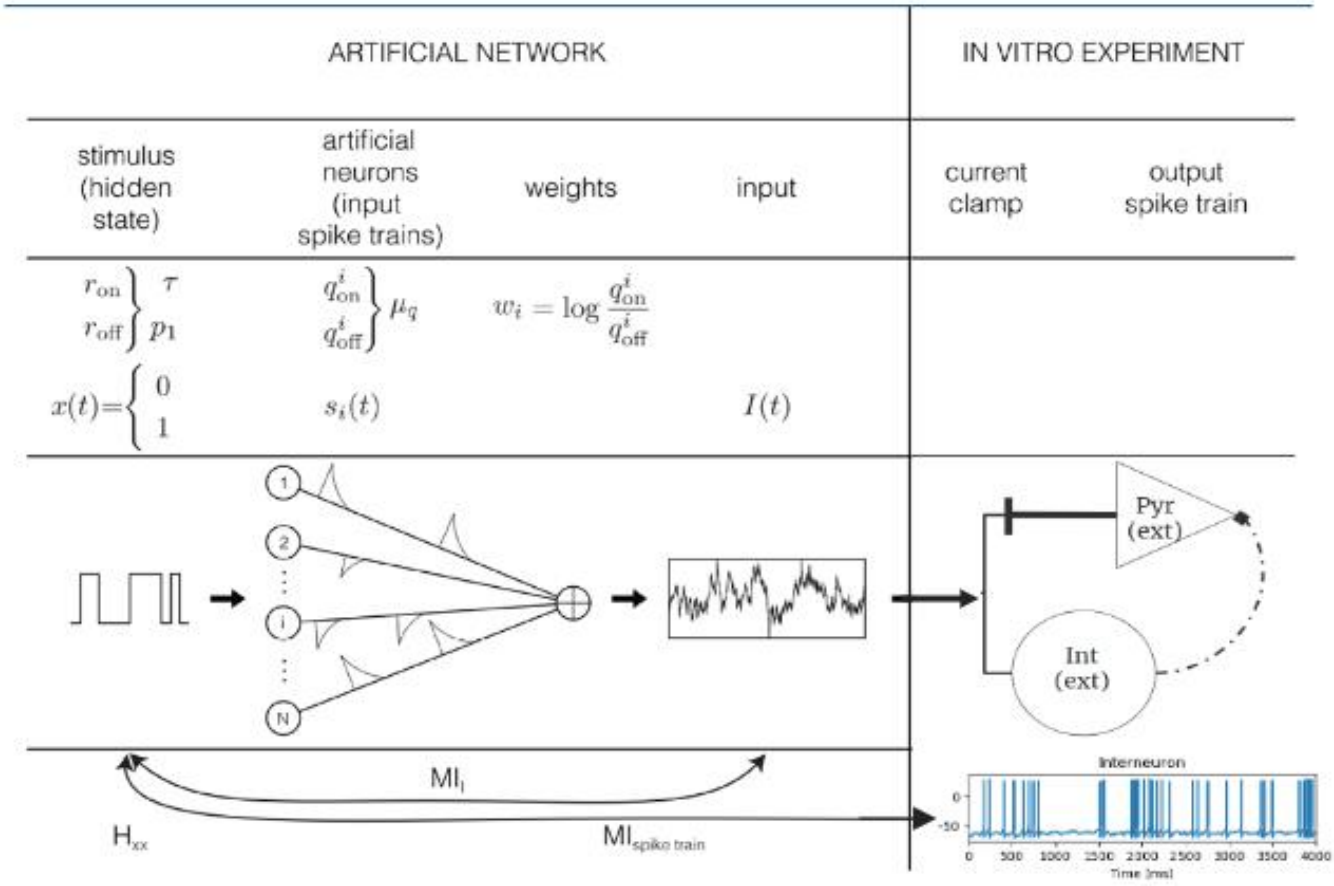

Fig. 4. Graphical Representation of Frozen Noise Input: it uses N artificial neurons that produce Poisson spike trains at rates qi_on and qi_off. These rates change based on a hidden Markov model with rates ron and roff. This generated current is injected into hippocampal pyramidal cells in a lab setting using a current clamp method. The spike trains that result from this are recorded and then used to reconstruct the hidden state of the model (Zeldenrust et al. 2017)

(Reprinted from Estimating the Information Extracted by a Single Spiking Neuron from a Continuous Input Time Series (Zeldenrust et al. 2017), Copyright 2017 by Frontiers in Computational Neuroscience. Reprinted with permission.)

2.2. Spikes and Bursts Classification:

There two forms of response the PC generates in corrospondence to dendritic input – spikes and bursts. According to the explanation given by Zeldenrust & Wadman (2012), the classification is based on the following criteria:

- A spike is a single action potential detected by a 0 mV threshold crossing in the pyramidal cell soma membrane (Fig. 2 (b))
- A burst consists of a series of high-frequency action potentials, where the first action potential has a much larger amplitude than the subsequent ones and are below the 0mV threshold (Fig. 2. (c))
- During a burst, the dendritic membrane potential is more depolarized compared to a spike.

2.3. Verification of the implementation of the neuron models:

The models were simulated on the Brian Simulator. The parameter values and expressions of equations were all based on values given the Zeldenrust & Wadman (2012) study. The correctness of the two-compartment PC was verified by checking whether the activity adheres to the bifurcation diagram (Fig. 3). The PC was stimulated with varying dendritic currents and its bursting and spiking activity was verified to follow the bifurcation plot. (Refer to plot (1) in the appendix)

2.3.2. Simulations:

A total of two types of simulations were run for a period of 180 seconds of simulation time. For both the simulations, the conductance of the synapse (*gsyn*) was varied between 2mS, 4mS and 8mS and the delay values in the synapse was varied between 0ms to 5ms in steps of 0.5ms making it a total of 33 simulations per conductance and delay value. The first type of simulation is for fast somatic inhibition wherein the interneuron projects to the soma of the PC and the input current is given to the dendrite compartment (following fast kinetics). The second simulation type is for dendritic inhibition wherein the interneuron projects to the dendrite of the PC and the input current is given to the soma compartment (following slow kinetics). Separate data files for every simulation were created and saved.

The two simulations are different in the sense of the simulating both the possible connections in a feedforward circuit however the overall goal is still to observe the effect on the theta rhythms with respect to the delays introduced per conductance value.

3. Analysis:

The key analysis conducted are:

3.1. Calculation of firing rates

To calculate the firing rates of the PC, we first extracted the spike time vector from the simulation data. We then divided the total number of spikes observed by the total duration of the simulation time to determine the overall firing rate of the PC.

3.2. Inter-Spike Interval calculations

To assess the regularity of firing patterns, we calculated the inter-spike intervals (ISI) for the PC. We used the differences in spike times between consecutive spikes to derive the ISI histogram and computed a threshold to distinguish between long and short ISIs. The distinction between spikes and bursts was made based on this threshold, identified as the lowest point in the ISI histogram. This index was chosen as the threshold to determine long and short ISIs. From the simulated data, we observed that bursts lasted at least 10 ms -15 ms, and there was at least a 100 ms difference between two spikes. Thus, to determine the number of spikes and first spikes in bursts, we considered an ISI greater than 100 ms as a single spike, and an ISI greater than 100 ms followed by an ISI less than 100 ms as the first spike in a burst. Based on this, we calculated the fraction of single spikes and the fraction of spikes in bursts (out of the total number of ISIs). We subsequently calculated their firing rates by dividing the number of single spikes by the total simulation time for the firing rate of single spikes, and the number of first spikes in bursts by the total simulation time for the bursting firing rate.

3.3. Power Spectrum and Impedence

We analyzed the power spectrum of the PC's membrane potential time series to identify the dominant frequencies present in the network dynamics. Additionally, we computed the impedance of the PC to quantify its frequency-dependent response characteristics. The power spectral densities were calculated using 3-second windows of membrane potential, which were then multiplied by the sampling frequency to improve the spectral resolution and reduce noise. Specifically, we focused on the subthreshold membrane potentials, using a threshold of -20 mV to isolate subthreshold activity. The power was computed using the Welch method from the Python SciPy library (Virtanen et al., 2020), which was also applied to the input current. From these spectra, we derived the impedance by dividing the subthreshold membrane potential PSD by the input current PSD. This impedance function provides insight into the PC's resistance to voltage changes across different input frequencies, revealing its frequency-dependent response properties.

3.4. Cross-Correlograms

To investigate the temporal relationship between the input current and PC, we computed their cross-correlograms. The correlation was made between the spike times of the PC, which was first converted into a binary signal, and the hidden states of the input current. The presence of a spike is represented as 1 and its absence as 0.

For the input current, the approach is based on the assumption of the frozen noise protocol, which posits that neurons respond to the presence or absence of a preferred stimulus feature, represented by a binary hidden state variable x. When x = 1, it indicates the presence of the stimulus, and when x = 0, it indicates its absence. By correlating the binary spike train of the PC with the binary signal of the hidden states, we were able to determine their temporal relationship. This analysis was performed across all synaptic conductance and delay conditions to gain a comprehensive understanding of the underlying dynamics. We also computed cross-correlations between the interneuron spike times and PC spike times. However, this analysis is not included in the main results section, as the analysis was unverified, but is present in the appendix (plot (2)).

4. Results:

Interneuron and Pyramidal Cell:

The activity of the PC and interneuron was first investigated without a synaptic connection. As seen in Fig. 2, the PC exhibits either a single spike or burst response. Whether the response remains a single spike or develops into a burst is determined immediately after the initial spike. Increased excitation leads to a burst, while inhibition prevents the burst and restricts the response to a single spike (Zeldenrust & Wadman, 2009; Zeldenrust & Wadman, 2012). The results focus on the activity of the PC, as the simulations varied the synaptic conductance *gsyn* values at 2mS, 4mS, and 8mS, and the synaptic delays from 0ms to 5ms in 0.5ms increments, to assess the impact on the PC's firing patterns.

4.1 Somatic Inhibition:

When the interneuron provides inhibitory input to the soma of the PC, the interneuron's firing pattern directly shapes the PC's output. With fast somatic inhibition, the firing rate of the PC does not increase as a function of increased synaptic conductance and delay. Instead, we found that the total event rate and the spike rate of the PC decreases, whereas the burst rate of the PC increases. This suggests that the strong and rapid inhibition from the interneuron onto the soma of the PC has an influence on its firing dynamics, favouring a bursting mode of operation over isolated spike firing (Fig. 5 (a) & (b)).

4.1.1. The firing patterns of pyramidal cell:

The firing rate analysis of the PC reveals that its overall firing rate decreases with increasing delays. When the first delay of 0.5ms is introduced, the firing rate dips and then slowly increases, but does not exceed the rate observed without any delays, eventually stabilizes at a relatively lower rate. Interestingly, for a conductance value of 8mS, the firing rate takes another dip at a delay of 1.5ms before gradually increasing again. This could be due to higher rate of occurrence single spikes (as also in Fig. 5 (d) & Fig, 15 (a)) for that delay value. Except for the condition of gsyn=8mS and delays between 0.5ms to 1.5ms, the burst rate of PC exhibits a different trend – it increases steadily as the delays are increased indicating that the bursting mode of PC becomes more prominent with longer delays.

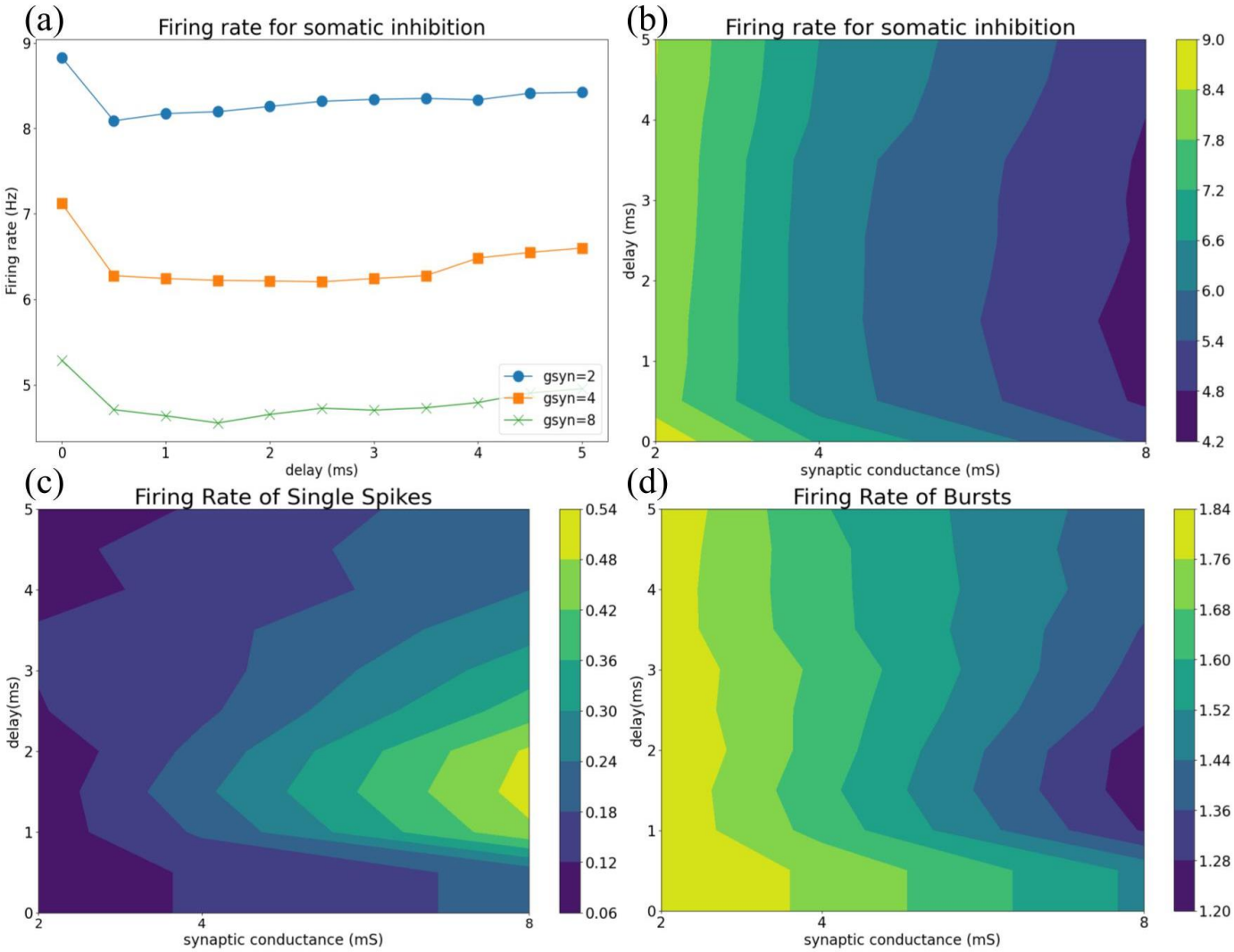

Fig. 5. (a) Line plot of firing rate of Pyramidal Cell plotted as a function of synaptic conductance and delays. We can observe the first dip at delay 0.5ms. (b) Heatmap representation of the firing rates as a function of synaptic conductance and delay depicting the decrease in rate as the synaptic strength. (c) Firing rate of isolated spikes reducing as function of conductance and delay. We can observe the singular condition of conductance value of 8mS and delays between 1ms to 2ms wherein the occurrence of isolated spikes is the highest. increases (d) Firing rate of isolated bursts following a similar trend as single spikes.

The inter-spike interval histogram of the PC's spike train displays a clear bimodal distribution, with distinct peaks corresponding to short and long ISIs (Fig. 6. (a)) The secondary peak, associated with the longer ISIs, is noticeably smaller in density compared to the primary peak of shorter ISIs. This bimodal pattern in the ISI distribution suggests that the delays in somatic inhibition exerted by the interneuron onto the PC preferentially triggers burst firing over the generation of isolated single spikes. This observation helps explain the overall reduction in the PC’s total firing rate that is observed despite the longer delays in the inhibitory input from the interneuron. Specifically, the bursts of action potentials contribute fewer individual spikes to the total spike count compared to the occurrence of isolated, single spike responses, thereby leading to the decreased PC firing rate as the inhibitory delay is increased.

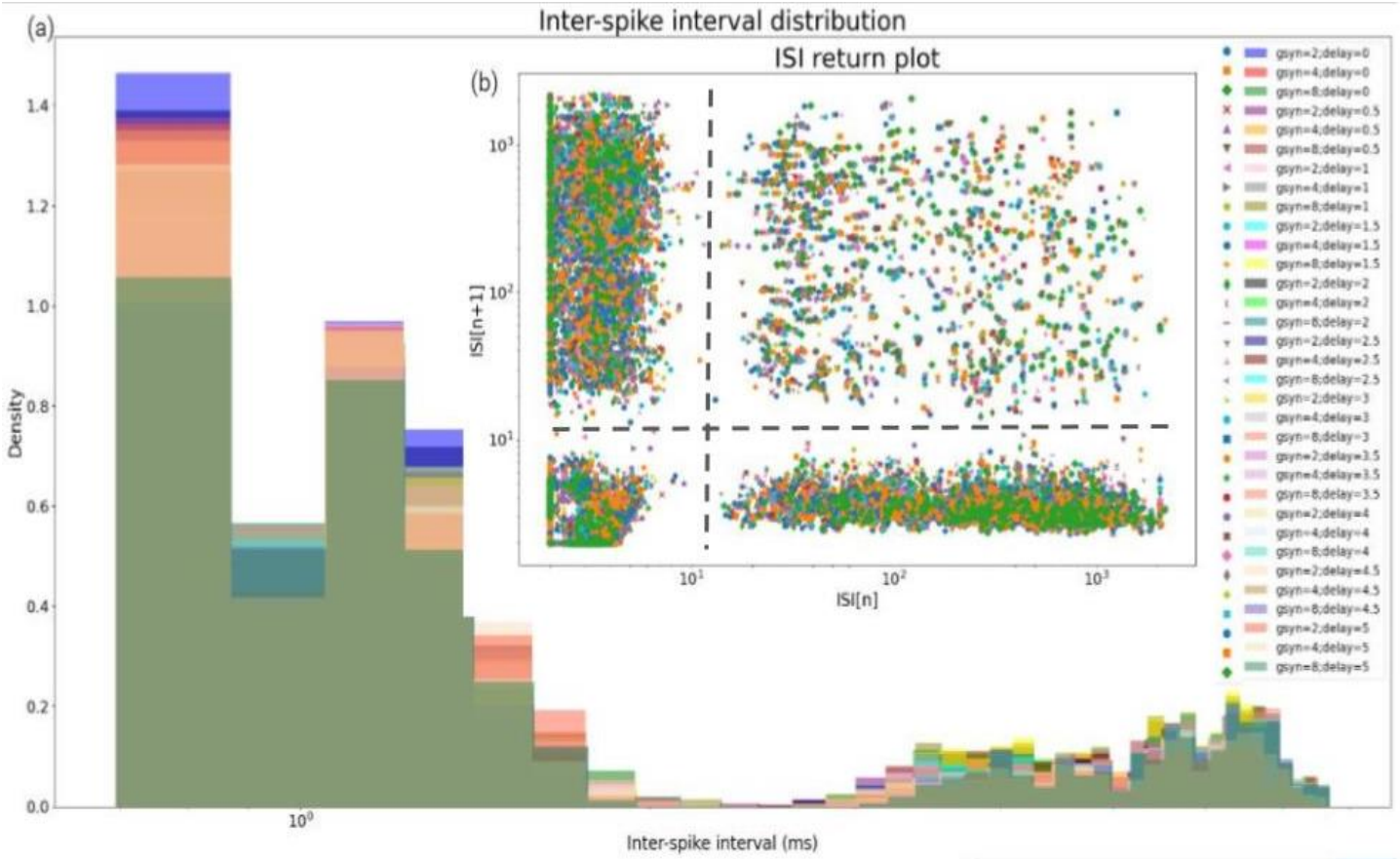

Fig. 6. (a) Inter-spike interval histogram showing a bimodal distribution of short and long inter spike intervals determined by the criteria if the interval between the previous spike and next spike is greater than 100ms, then its a single spike, if its less than 100ms then its a burst (b) return plot shows clear clustering of data. The left most quadrants representing short ISIs and the right most quadrants representing long ISIs, majority of the points falling at the left most quadrants indicating a dominance of bursting activity.

Quantitative analysis of the heatmap and line plot visualizations depicting the isolated spike and burst firing rate dynamics of PC reveals distinct patterns that emerge as a function of the synaptic conductance values. Specifically, for the higher conductance conditions, for gsyn=8mS, the introduction of temporal delays ranging from 0.5ms to 1.5ms between the interneuron and PC's synaptic connection results in an increase in the single spike firing rate of the PC.

This elevated single spike rate reaches a peak of 0.54 Hz, as observed by the warmer colors regions on the heatmap. Further supporting this observation, the single spike percentage metric indicates that at these delay values, the PC exhibits a greater propensity for generating isolated, single action potentials rather than burst firing responses, especially when compared to the lower conductance condition of 2 mS (Fig. 7 (a) & (b)). This trend of increased single spiking is also observed for the intermediate 4 mS conductance case. However, in stark contrast, for the lowest 2 mS conductance value, the PC demonstrates a greater tendency to fire bursts rather than emitting individual spikes under the influence of the delayed inhibitory input from the interneuron.

The return plot further confirms the distinct clustering of data points corresponding to the long and short ISIs observed in the PC's spike train, with the majority of points congregating at the lower interval values (Fig. 6. (b)). This clustering pattern is indicative of a predominance of burst-firing responses over isolated single spikes. This finding directly corroborates and aligns with the bimodal distribution characteristics revealed through the ISI histogram analysis

Taken together, the evidence suggests that even with the introduction of temporal delays in the inhibitory input from the interneuron, somatic inhibition remains a robust and influential in shaping the PC's firing dynamics. Specifically, the interneuron's inhibitory influence appears to effectively suppress the PC's activity, favouring the generation of burst-firing responses over the emission of isolated single action potentials, particularly under conditions of higher synaptic conductance values. However, the specific quantitative effects of systematically varying the delay between the interneuron and PC on the relative proportions of single spike versus burst firing rates exhibit more nuanced and complex patterns, demonstrating differential trends depending on the particular synaptic conductance regime being examined.

4.1.2. Power Spectral Analysis:

The power spectral density (PSD) analysis of the simulated local field potential signals (i.e. membrane potentials) provides further insights into the emergent oscillatory dynamics that arise from the modulation of the temporal delay and synaptic conductance between the interneuron and PC. As the delay between the interneuron and PC is increased from 0ms to 5ms, for the higher synaptic conductance conditions of 4 mS and 8 mS, the overall power of the PSD curve is observed to decrease, while the dominant peak frequency remains relatively unchanged (Fig. 8 (b)). This finding suggests that the introduction of greater temporal delays in the inhibitory input from the interneuron to the PC results in a dampening of the oscillatory power present in the sub-threshold membrane potential, without fundamentally altering the underlying frequency content of these network-level neural rhythms. The decrease in power with increasing delay points to a disruption in the precise temporal coordination of inhibitory and excitatory inputs acting upon the PC, which in turn perturbs the synchronization of spiking activity within the local circuit. Majority of the power seems resides in lower frequency band, which means that the neurons are at a low pass filter. However, the persistence of the dominant frequency peak in the PSD indicates that the fundamental frequency of the oscillatory dynamics is maintained, despite the attenuation in overall power.

Collectively, these observations tell us how modulations in the inhibitory-excitatory balance and temporal dynamics within neural microcircuits could possibly shape the emergent rhythmic activity patterns reflected in the local field potential. In contrast for lower conductance of gsyn=2mS, the down trend is not observed. Instead, the overall the PSD remain relatively stable.

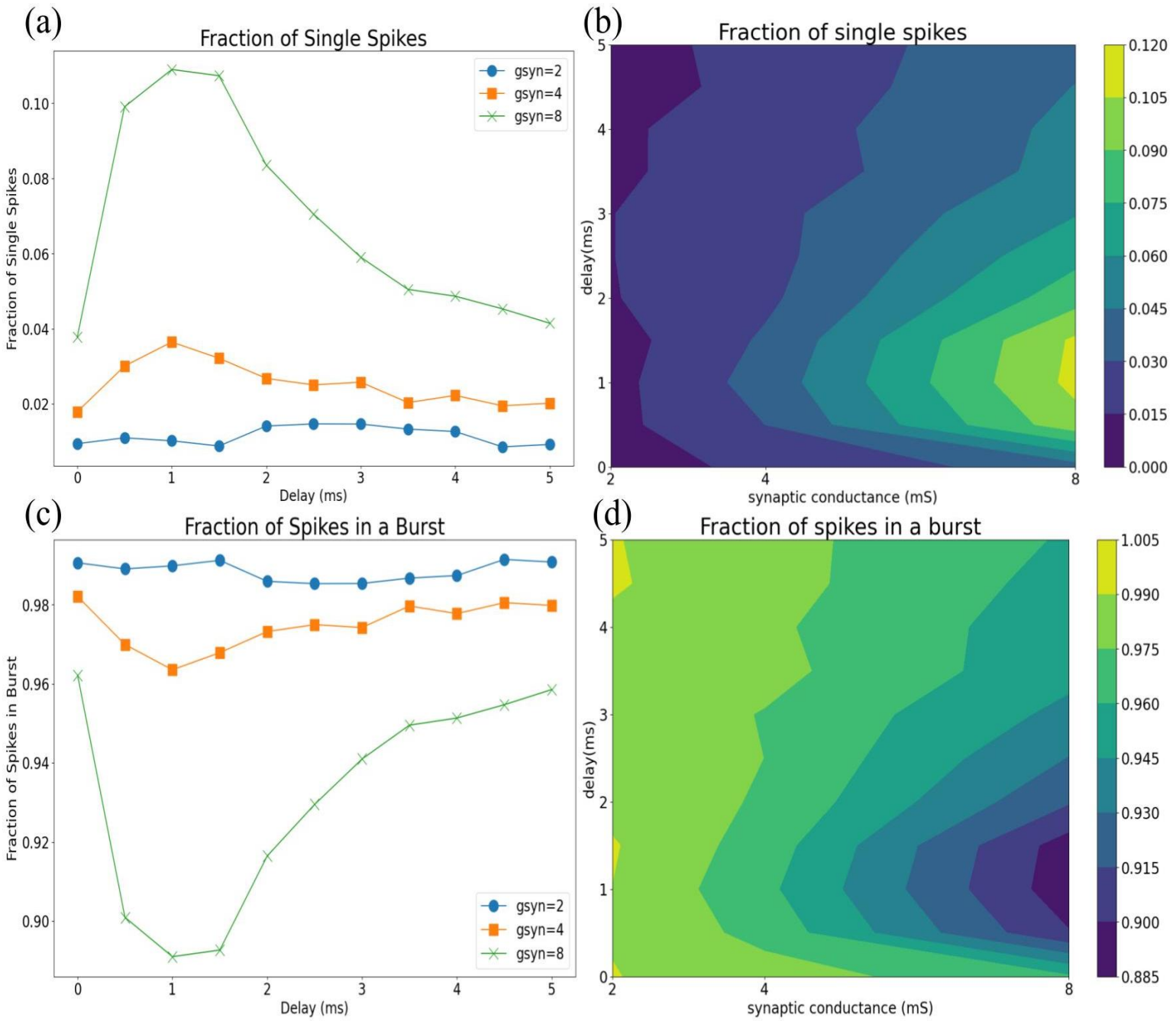

Fig. 7. (a) line plot of single spikes calculated as number of single spikes / total number of spikes. (b) heatmap representation of (a) (c) line plot of spikes in burst calculated as the (total number of spikes – total number of single spikes) / total number of spikes (d) heatmap representation of the same.

The impedance analysis shows that the resistance decreases as a function of higher synaptic delay and conductance values (Fig. 8. (c)). This is complementary to the downtrend observed for PSD of sub-threshold potentials. This reduction in oscillatory power is accompanied by a corresponding decrease in the impedance i.e. resistance to voltage, which becomes more pronounced under conditions of higher synaptic conductance and temporal delay.

The decrease in resistance could be indicative of higher propensity for burst firing in PC, as the inhibitory influence from the interneuron becomes more temporally dispersed and attenuated.

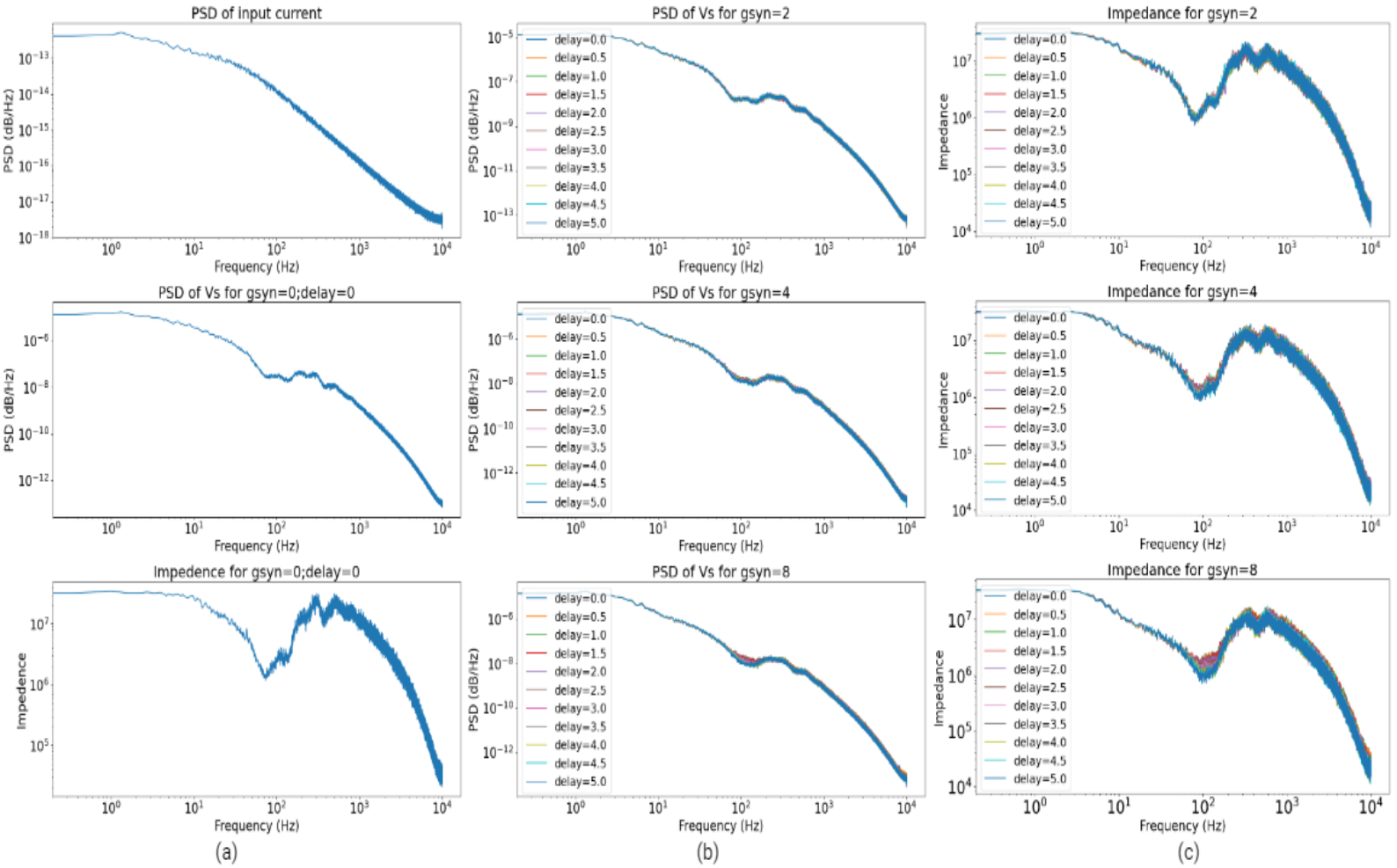

Fig. 8. (a) From top to bottom: Power Spectrum of input current, sub-threshold membrane potentials and impedance calculated as power of input current / power of membrane potentials for control condition wherein there is no synapse and delay between PC and interneuron. (b) From top to bottom: Power Spectrums of sub-threshold membrane potentials of varying synaptic conductance and delays values. For gsyn=8mS we observe the downtrend in power. (c) From top to bottom: impedance of varying synaptic conductance and delay values calculated as power of input current / power of membrane potentials for every respective condition. For gsyn=8mS we observe similar downtrend indicating lowering of resistance for longer delays.

4.1.3. Correlogram:

The cross-correlation analysis between the PC's binary spike train and the hidden states derived from the input current shows that as the temporal delay between the interneuron and PC is increased, the correlation between the PC's spiking activity and the hidden states decreases. Notably, the presence of a positive lag in this cross-correlation suggests that the PC's spike times tend to weakly follow the hidden state signal. This observation implies that the inhibitory influence exerted by the interneuron is attenuated or depressed as the delay is increased (Fig. 9.) Importantly, the low correlation values themselves indicate a relatively weak positive correlation between the PC's spiking and the hidden states. This indicates that the PCs spike times only weakly track or follow the hidden state. This weak positive correlation suggests that the delay in inhibition disrupts the precise temporal coordination between inhibition and excitation within the local circuit, culminating in a desynchronization of the neural activity.

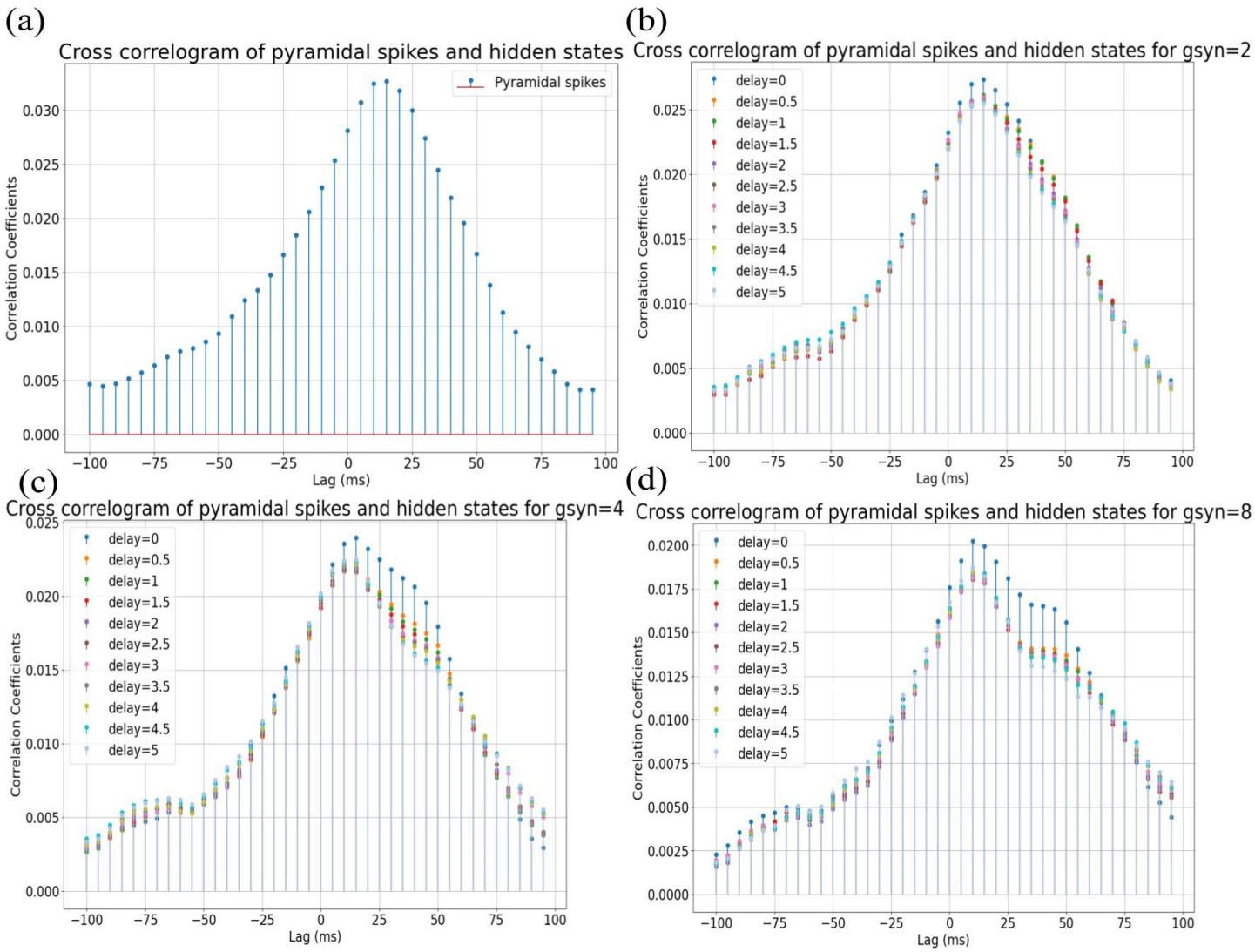

Fig. 9. (a) Correlogram between PC and input current when there is no synapse and delay i.e. when the PC is by itself. (b) (c) & (d) Correlogram between PC and input current for varying conductance value of 2mS, 4mS and 8mS and varying delays respectively.

4.2. Dendritic Inhibition:

When the interneuron provides inhibitory input to the dendrite of the PC, the inhibition appears to be less effective in suppressing the PC spiking activity compared to somatic inhibition. With slow dendritic inhibition, the firing rate of the PC increases as the synaptic conductance and temporal delay between the interneuron and PC are increased. Specifically, we found that while the overall total event rate and individual spike rate increase under these conditions, the rate of burst firing by the PC decreases. This suggests that the delayed inhibitory influence from the interneuron favours the generation of isolated spikes in PC over burst responses particularly when the synaptic conductance is higher.

4.1.4. The firing patterns of pyramidal cell:

The analysis of the PC's firing rate dynamics is observed to increase as the delay is incrementally raised for every synaptic conductance. Interestingly, this general upward trend is marked by a dip in the firing rate when the first delay value of 0.5ms is introduced, after which the firing rate subsequently increases from that point onward (Fig. 10 (a)).

When examining the specific behavior of single spike generation for a conductance value of 8 mS, PC's rate of single spike generation for that conductance exhibits a linear decline as the delay is increased up to 3ms (Fig. 12. (a)). At delay of 3,5ms, the single spike rate increases before declining once again. Notably, the firing rate at 3.5ms delay point also decreases slightly before rising back up. This pattern suggests that the PC may have a particular preference for firing single spikes for this delay value, even if the resulting ISIs are quite long. The underlying mechanisms driving this selectivity for single spike generation at this delay value suggest the inhibition from the interneuron becomes less effective in supressing PC's spiking allowing it to fire at lower overall rates but with a higher propensity for single spikes.

The ISI histogram exhibits a clear bimodal distribution, with distinct peaks corresponding to long and short inter-spike intervals (Fig. 12. (a)). The bimodal pattern suggests that dendritic inhibition appears to trigger a mix of isolated spikes and spike bursts, rather than predominantly one or the other. The well-distributed second peak of the bimodal distribution indicates that the PC exhibits a less propensity for burst firing when delays are increased.

Further analysis of the heatmap and line plots depicting the firing rate of single spikes and bursts was done. For a higher synaptic conductance value of gsyn=8mS, the introduction of delays ranging from 0.5ms to 1.5ms increases the firing rate of single spikes in the PC, reaching a peak value of 1.08 Hz as shown by the warmest color on the heatmap (Fig. 10. (c)). This suggests that the delayed inhibitory influence from the interneuron promotes more isolated, single spike generation in the PC under higher conductance conditions and shorter delays.

This shift may have important implications for understanding how the temporal coordination between inhibition and excitation within the local neural circuit shapes the emergent rhythmic activity patterns, including potential modulations in the synchronization of theta oscillations, which is the focus of the main research question.

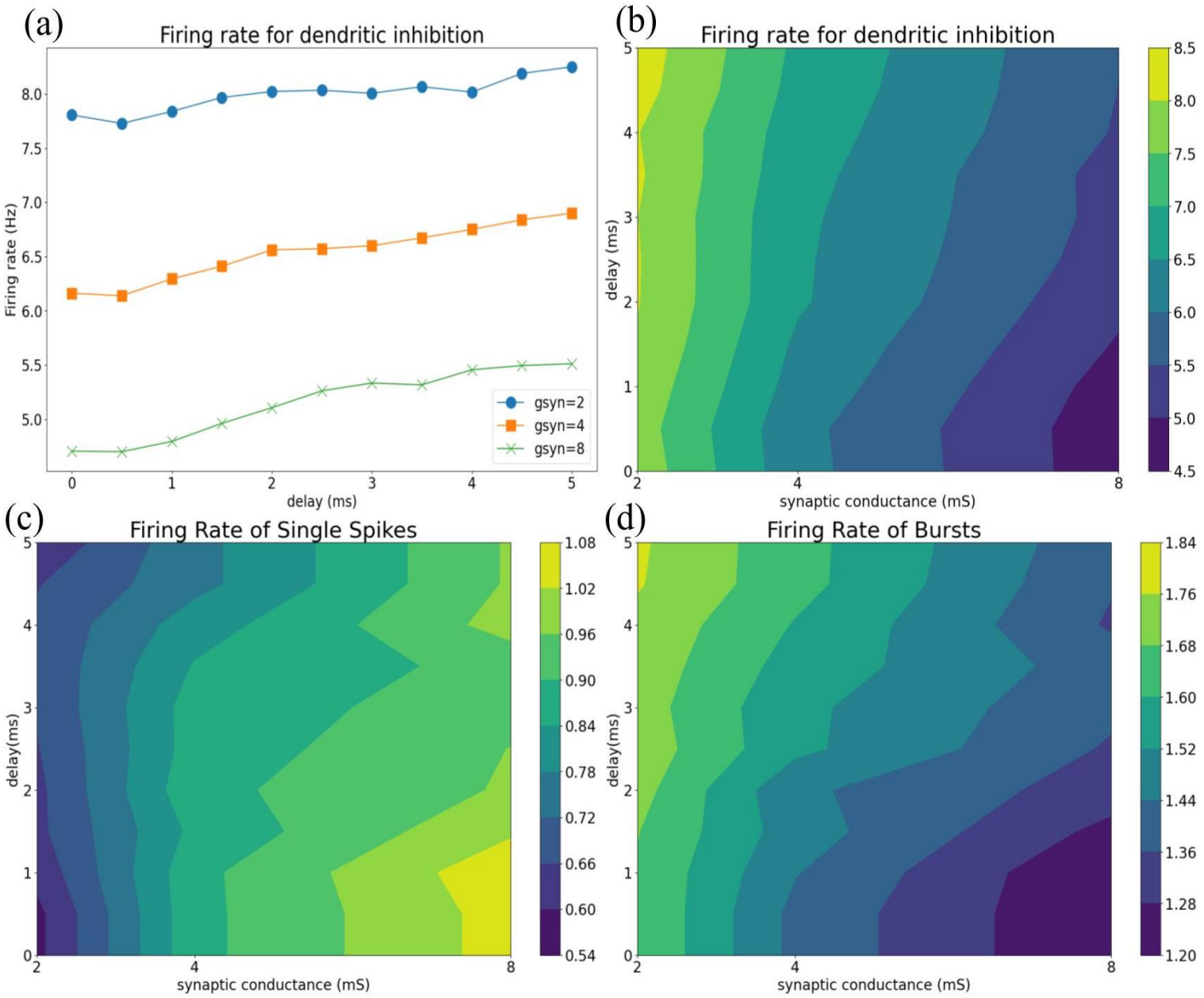

Fig. 10. (a) Line plot of firing rate of Pyramidal Cell plotted as a function of synaptic conductance and delays. (b) Heatmap representation of the firing rates as a function of synaptic conductance and delay depicting the increase in firing rate as the delays become longer (c) Firing rate of isolated spikes increases as function of conductance and delay. (d) Firing rate of isolated bursts follows the opposite trend wherein the rate reduces for higher conductance values

The return plot shows distinct clusters of both long and short ISIs. The pattern suggests that the dendritic inhibition from the interneuron triggers a mix of isolated spikes and spike bursts in the pyramidal cell, rather than predominantly one or the other.

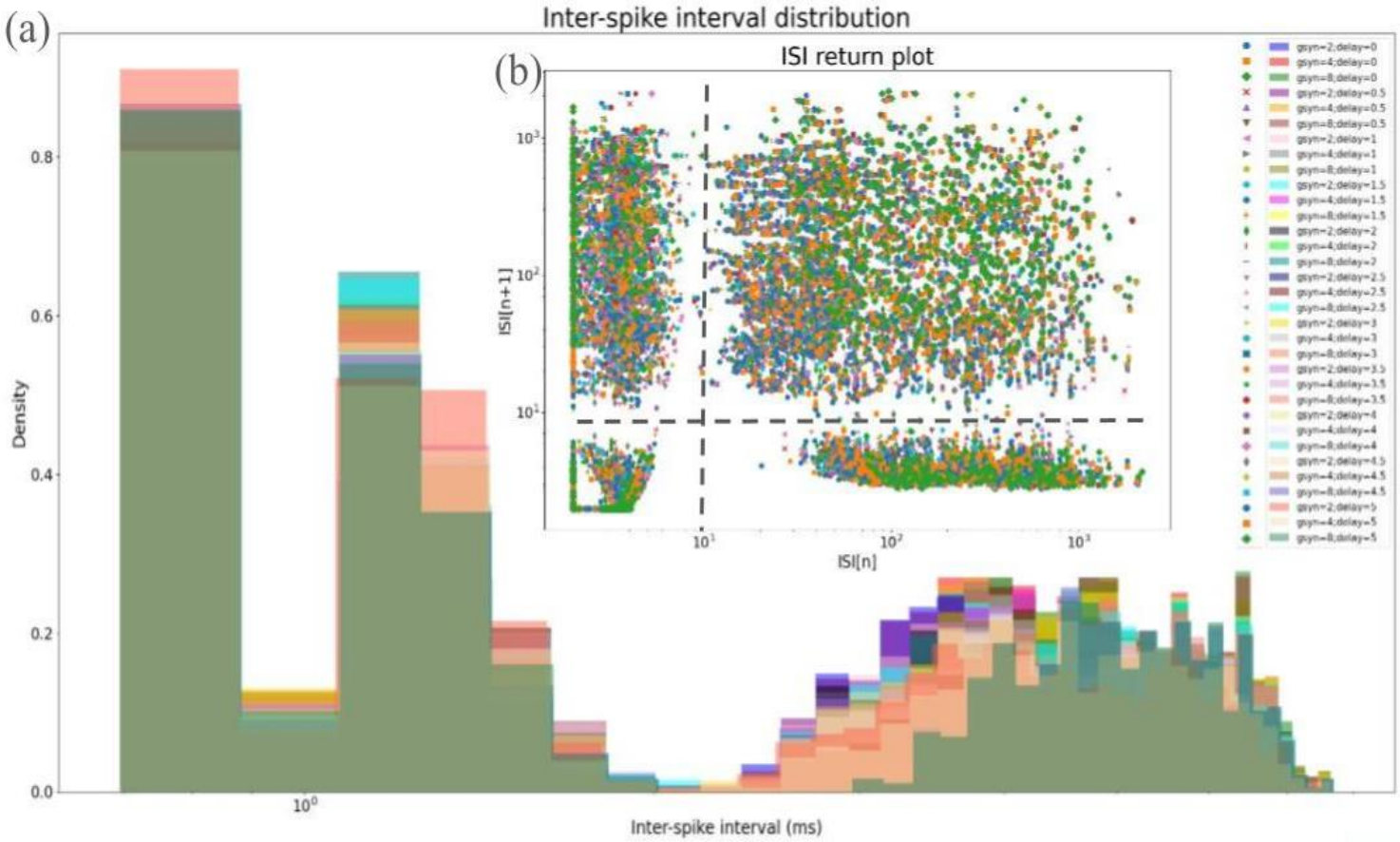

Fig. 11. (a) Inter-spike interval for dendritic inhibition histogram showing a bimodal distribution of short and long inter spike intervals determined by the criteria if the interval between the previous spike and next spike is greater than 100ms, then its a single spike, if its less than 100ms then its a burst (b) return plot shows clear clustering of data. The left most quadrants representing short ISIs and the right most quadrants representing long ISIs.

Furthermore, the observation that the PC's firing rate increases with incrementally longer delays in the inhibitory input indicates that dendritic inhibition becomes less effective at suppressing the PC's spiking activity as the temporal mismatch between excitation and inhibition increases. This points to a disruption in the precise temporal coordination between inhibition and excitation within the local circuit, indicating desynchronization of the neural activity.

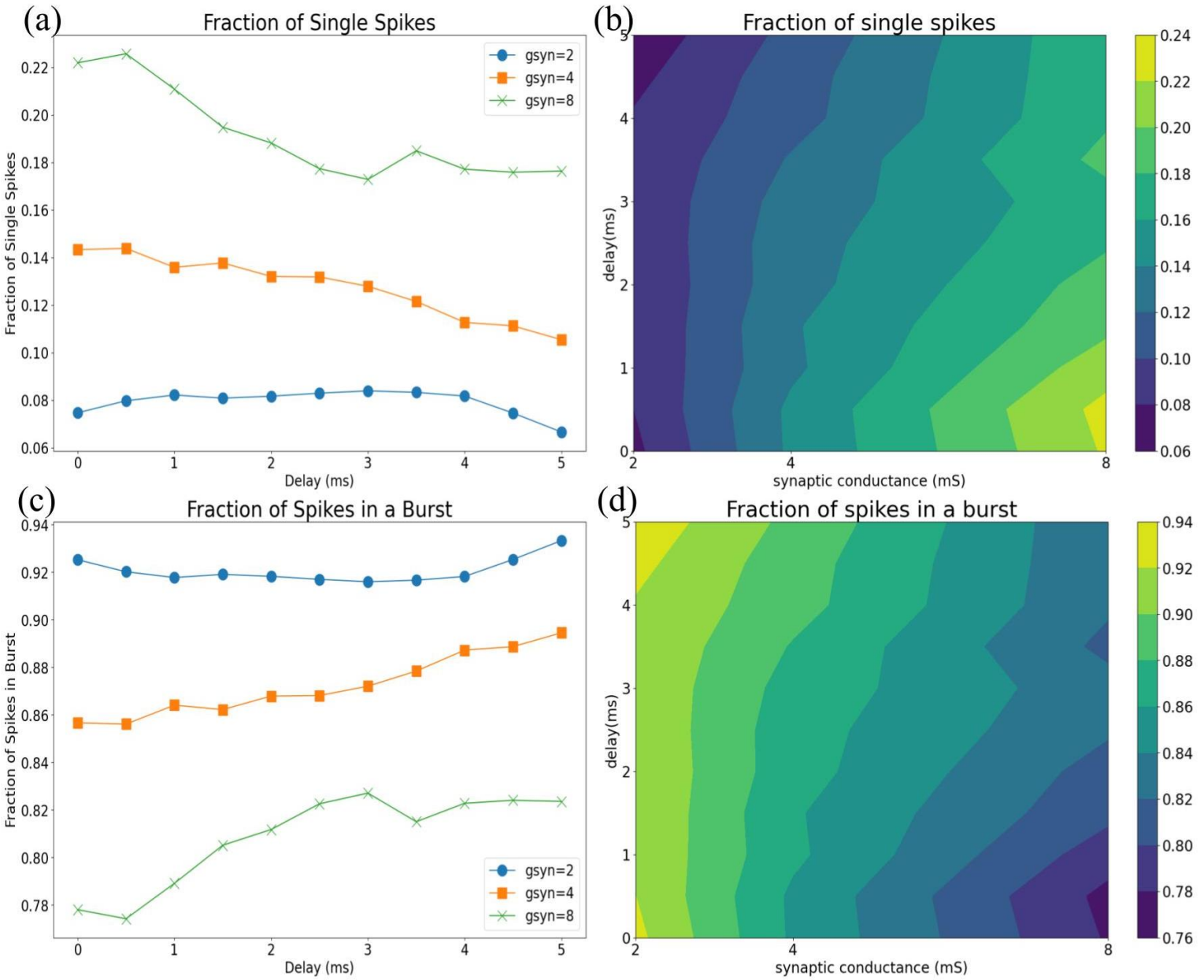

Fig. 12. (a) line plot of single spikes calculated as number of single spikes / total number of spikes. Here we observe the increase in single spikes for gsyn=8mS between delays of 3ms to 4ms (b) heatmap representation of (a). Here as well we see a peak in warmer color for the same condition (c) line plot of spikes in burst calculated as the (total number of spikes – total number of single spikes) / total number of spikes (d) heatmap representation of the same.

4.1.5. Power Spectral Analysis:

The PSD analysis was conducted on the PC's subthreshold potentials for varying synaptic conductance and temporal delays, similar to the analysis done for somatic inhibition. The results showed that the PSDs for the subthreshold potentials did not exhibit any notable differences in power compared to the PC's responses in the absence of any inhibitory inputs (Fig, 13 (b)). Similarly, the impedance analysis indicated that the resistance to these subthreshold potentials remained relatively minimal across the different conditions (Fig, 13 (c)). These findings suggest that the dendritic inhibition had a limited impact on the overall subthreshold dynamics of the PC, in contrast to the more pronounced effects observed on the PC's spiking activity patterns.

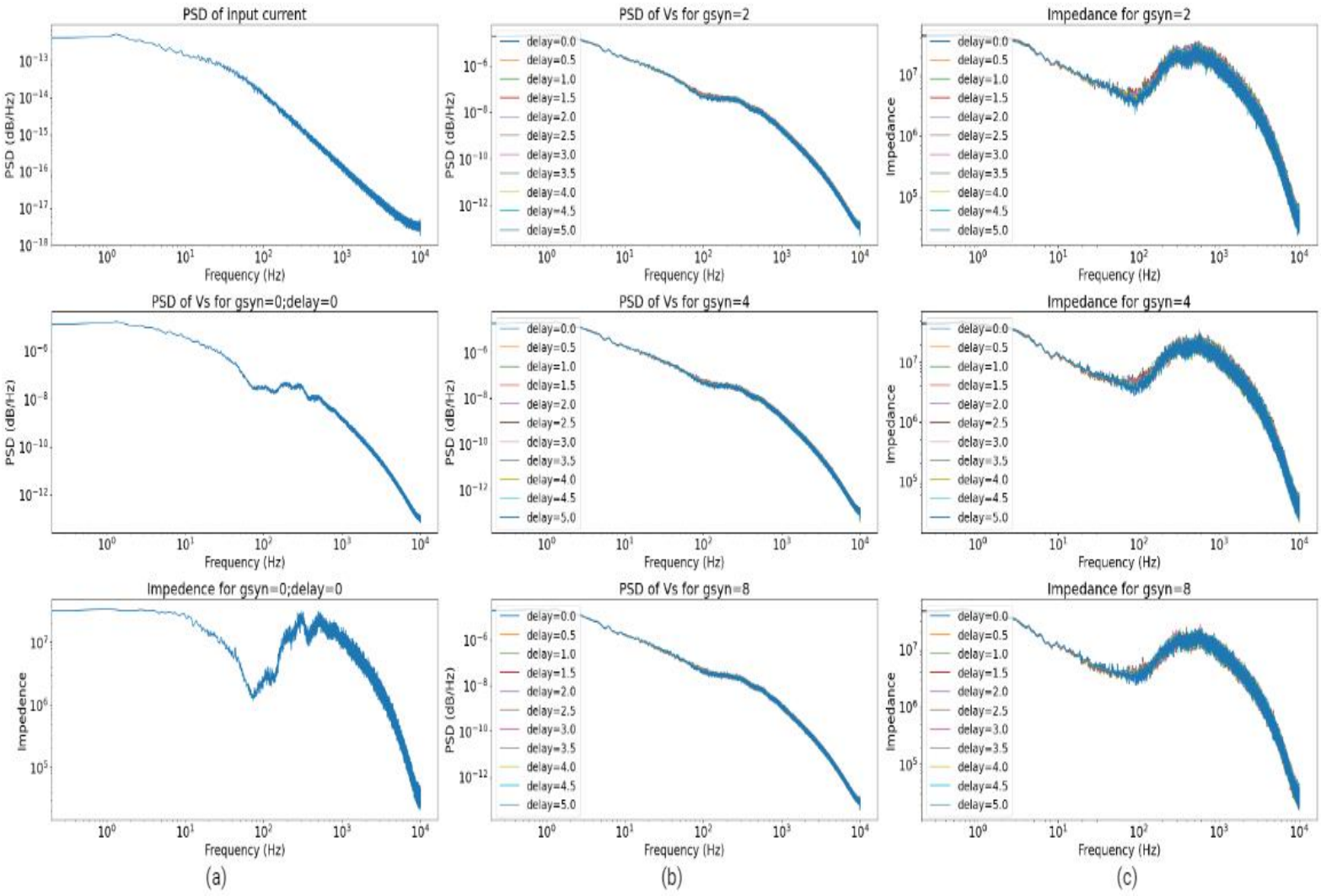

Fig.13. (a) From top to bottom: Power Spectrum of input current, sub-threshold membrane potentials and impedance calculated as power of input current / power of membrane potentials for control condition wherein there is no synapse and delay between PC and interneuron. (b) From top to bottom: Power Spectrums of sub-threshold membrane potentials of varying synaptic conductance and delays values (c) From top to bottom: impedance of varying synaptic conductance and delay values calculated as power of input current / power of membrane potentials for every respective condition.

4.3.3. Correlogram:

Similar to the analysis for somatic inhibition, the cross-correlation analysis between the PC's binary spike train and the hidden states derived from the input current was performed. Although the correlation values are low, there appears to be an even more pronounced decrease in correlation for higher synaptic conductance values of gsyn=8mS and longer delay conditions, with the correlation approaching small negative values at the more positive lag times (Fig, 14 (d)). This suggests that the temporal mismatch introduced by the increased delays disrupts the relationship between the PC's spiking activity and the underlying hidden states representing the input current, potentially reflecting a desynchronization of the neural activity within the local circuit.

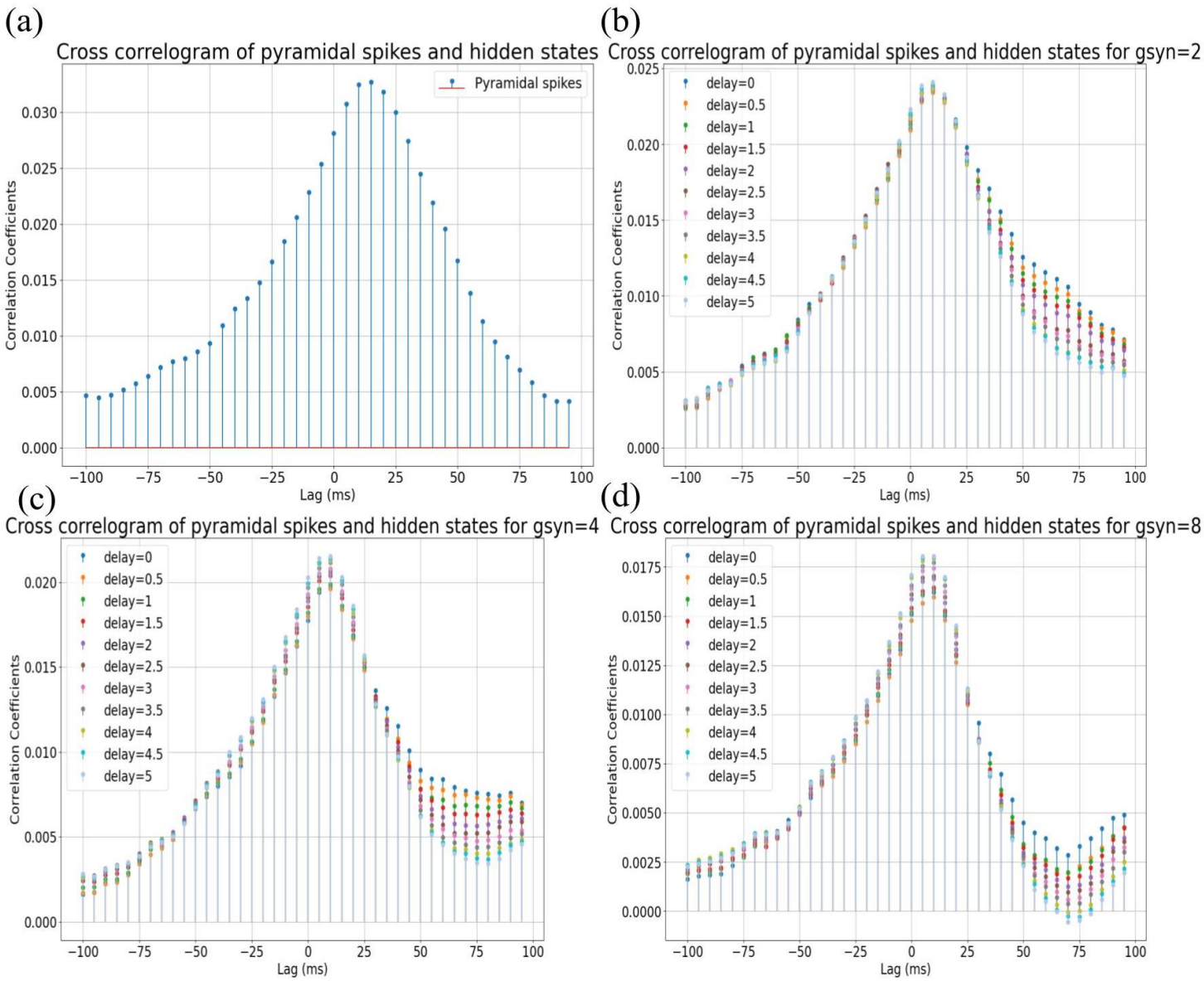

Fig.14. (a) Correlogram between PC and input current when there is no synapse and delay ie when the PC is by itself. (b) (c) & (d) Correlogram between PC and input current for varying conductance value of 2mS, 4mS and 8mS and varying delays respectively.

5. Discussion:

The key findings from this simulations study suggest that an increase in the delay of inhibition onto the soma of a PC still results in much effective inhibition as compared to dendritic inhibition. These changes can lead to a slowing down and potential disruption of theta rhythms generated within the local neural circuit, thus partially supporting our hypothesis. As mentioned in the Zeldenrust & Wadman (2012) study, burst and spike rates of PC can be independently regulated based on different points of connection in a feedforward circuit.

Feed-forward inhibition expands the dynamic range of the PC's input-output relationship (Ewell & Jones, 2010; Ferrante et al. 2009; Pouille et al., 2009; Wierenga & Wadman, 2003). Different types of inhibitory synapse sites whether in somatic or dendritic in feedforward (Zeldenrust & Wadman, 2012) or feedback (Zeldenrust & Wadman, 2009) circuit do not tend to exist exclusively but rather mutually co-exist. Both circuits trigger bursting and spiking activity which the brain processes differently (Zeldenrust & Wadman, 2012).

The classical view is that feed-forward inhibition dampens the output for prolonged stimuli by suppressing the signal after an initial transient response (Zeldenrust & Wadman, 2012). Additionally, feed-forward inhibition enhances the precision of spikes by narrowing the temporal window for firing (Jonas & Buzsaki, 2007; Mittmann et al. 2004; Pouille & Scanziani, 2001). A similar complex modulation of the PC's firing rate was observed when investigating the effects of varying the location, strength and synaptic delays of feedforward inhibition.

For somatic inhibition, the burst rate increases with increase in synaptic strength and delay except the case of gsyn=8mS and delay values from 0.5ms to 1.5ms. This was due to higher generation of spikes for that delay period as the IPSPs are 'not coming on time' anymore decreasing the effects of inhibition. This is the only condition wherein the spike rate of the PC is considerably higher compared to the other conditions. We observed a total of number of 100 single spikes for this condition (Fig, 15. (a)).

For dendritic inhibition the burst rate increases with increase in delays and synaptic strength and the single spike rate decreases. The only special condition of gsyn=8mS and delay=3.5ms shows an increase in single spikes, as compared to the other delays for that conductance value, we observed a total of 180 single spikes (Fig. 15 (b)). The increase of burst rate resulting in the increase of overall firing rate of the PC.

The overall effect of inhibition can be understood as a result of the after hyper-polarisation (AHP) current in the PC which has been investigated before in Booth & Bose (2001a) & Zeldenrust & Wadman (2009; 2012). As explained in a similar study by Zeldenrust &Wadman (2012) slow dendritic inhibition can stop or convert bursts into single spikes, reducing the AHP current in PC. This shortens the ISI, leading to an increase in the overall spike rate. In contrast, fast somatic inhibition is more effective at preventing spikes by inhibiting the spike-initiating site in the soma. The AHP current in PC causes a long refractory period after a burst causing a delay for the next activity. To generate a single spike, the dendritic calcium spike that induces a burst needs to be repressed, and this is easier with slow dendritic inhibition than fast somatic inhibition, due to the dendritic location of the calcium currents.

Therefore, fast somatic inhibition is less effective than slow dendritic inhibition in both generating single spikes and converting bursts into single spikes. Even though the focus of Zeldenrust & Wadman (2012) was on the filtering properties of interneuron, the effect on the PC is in line with the results in the present study. The only exceptions being the conditions of gsyn=8mS and delay from 1ms-2ms in somatic inhibition and gsyn=8mS and delay=3.5ms in dendritic inhibition. Similar to the Zeldenrust & Wadman (2012) results, our findings indicate that slow dendritic inhibition increases the spike rate of PCs, whereas fast somatic feed-forward inhibition does not induce a similar increase in spiking activity. This indicates the importance of spatiotemporal organization, as the inclusion of synaptic delay can produce very different effects on PC's firing patterns.

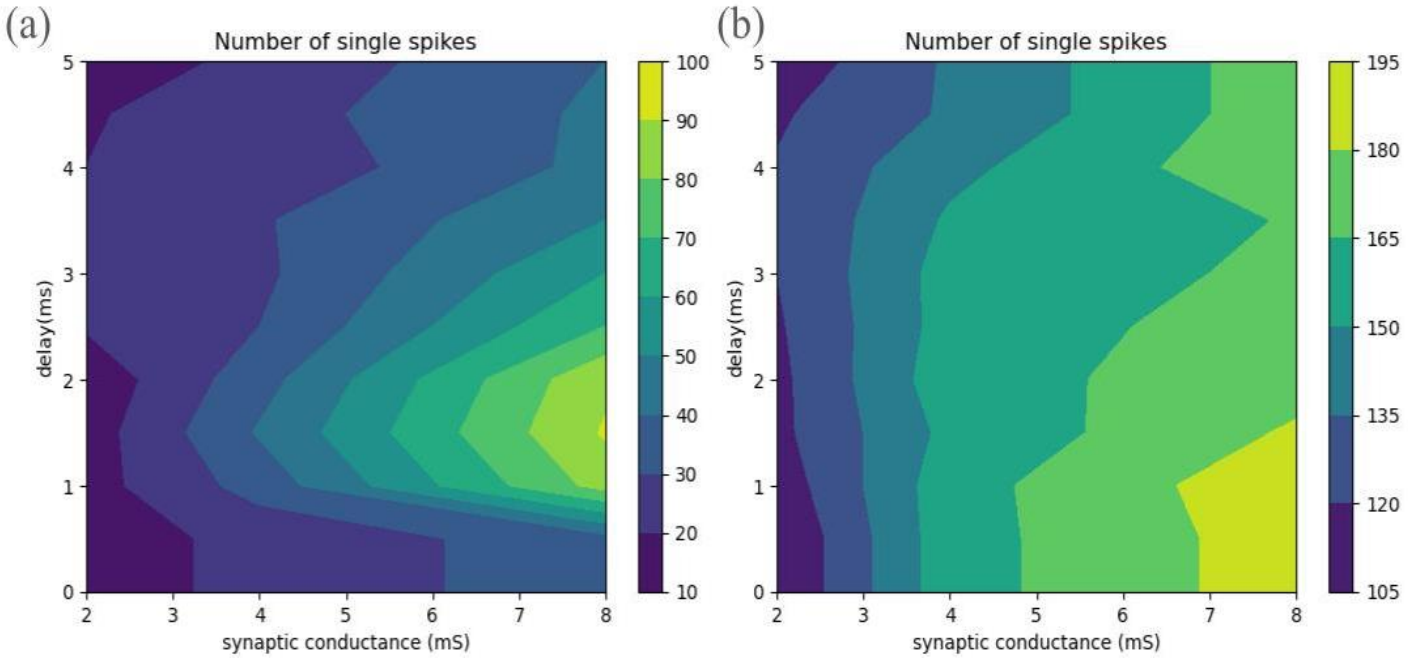

Fig.15. Heatmaps of number of single isolated spikes identified based on the inter spike intervals the criteria: if the interval between the previous spike and next spike is greater than 100ms, then it's counted as a single spike.

The findings from the Dubey et al. (2022) examined how delays in inhibition can impact the activity of PC and potentially disrupt theta rhythms making it relevant to the present study. To corroborate their findings, the present study also explored how temporal factors, such as synaptic delays, can alter the inhibitory control exerted by interneurons on the primary excitatory neurons. The decreased myelination and signal strength of PV+BC interneurons in the Dubey et al. (2022) study led to a decrease in the interneuron's inhibitory influence, resulting in an increase in slow brain waves. The present study also suggests that increased delays in inhibition onto PC can disrupt the normal synchronization of neural activity, potentially contributing to changes in theta oscillations. The results from Dubey et al. (2022) showed a precession in theta frequency with delay in inhibition as small as 0.5ms, but this effect only seems to hold true for dendritic and not somatic inhibition. In contrast, the present study finds that PCs tend to generate bursts at higher frequencies for somatic inhibition.

Even though the present study cannot verify the shift in theta oscillations precession, it can demonstrate the change in activity of the primary excitatory neuron with increasing delays and synaptic strength, which is indicative of a change in theta oscillations.

The analysis of power spectra and cross-correlations suggests that changes in the firing pattern of PC may indicate a shift in theta frequency. However, due to time constraints, conclusive analysis could not be performed to fully verify this hypothesis. To confirm the potential impact on theta frequency, further investigation is needed. This could be done by investigating spectrograms of the PC's sub-threshold membrane potentials and spike timing, which would help visualize any effects on theta oscillations. Additionally, a cross-correlation analysis between the PCs and interneurons would provide insights into the degree of synchronization and coupling between these neuronal populations. The results of this analysis are included in the appendix but were not incorporated into the main report, as they are unverified. Furthermore, the impedance should be calculated as the Fourier transformed sub-threshold potentials and input current. This was not implemented in the present study.

The initial motivation for this work was to understand how even small delays in inhibition could potentially affect theta frequency. To explore this, we set up a computational model and carefully verified its accuracy. The analysis then examined the effects of systematically varying synaptic delay and conductance on the inhibitory influence and spiking activity of the excitatory PCs. We observed clear changes in neuronal activity patterns as a function of the delay, with stronger synapses exhibiting more pronounced effects compared to weaker synaptic connections. Further in-depth exploration is needed to fully characterize the underlying changes in the bursting and single-spiking regimes of the PCs under different spatiotemporal patterns of inhibition. In conclusion, the findings suggest that subtle changes in the temporal dynamics of inhibitory input could potentially contribute to abnormalities in the theta rhythms observed in neurodegenerative disorders such as MS.

Appendix:

Parameters and Equations of the Neuron Models

1. Pyramidal Cell:

The pyramidal cell is modelled using Pinksy and Rinzel (1994) two compartment model. It has a soma compartment with membrane potential *Vs* and dendrite compartment with membrane potential *Vd*. The two compartments are coupled with conductance *gc*.

$$C_m\dot{V}_s = -I_{L,s} - I_{Na} - I_{K-DR} + \frac{g_c}{p}(v_d - v_s) + \frac{I_s}{p} - I_{syn,s} \quad (1)$$

$$C_m\dot{V}_d = -I_{L,d} - I_{Ca} - I_{K-AHP} - I_{K-C} + \frac{g_c}{1-p}(v_s - v_d) + \frac{I_d}{1-p} - I_{syn,d} \quad (2)$$

Equation (1) explains the dynamics of the soma compartment. $I_{L,s}$ is the leak current, I_{Na} is the sodium current, and I_{K-DR} is the delayed-rectifier potassium current. These currents are calculated as:

$$I_{L,s} = g_L\,(v_s - v_L)$$

$$I_{Na} = g_{Na}\,m_\infty^2(v_s)h(v_s - v_{Na})$$

$$I_{K-DR} = g_{K-DR}\,n(v_s - v_K)$$

Equation (2) explains the dynamics of the dendrite compartment. $I_{L,d}$ is the leak current, I_{Ca} is the calcium current, I_{K-AHP} is afterhyperpolarisation current and, I_{K-C} is the calcium induced potassium current. These currents are calculated as:

$$I_{L,d} = g_L\,(v_d - v_L)$$

$$I_{Ca} = g_{Ca}\,s^2(v_d - v_{Ca})$$

$$I_{K-AHP} = g_{K-AHP}\,q(v_d - v_K)$$

$$I_{K-C} = g_{K-C}\,c_X(Ca)(v_d - v_K)$$

The calcium concentration (Ca) is modelled as:

$$\dot{Ca} = -0.13I_{Ca} - 0.075Ca$$

The kinetics of the gating variables are calculated using the following equations:

$$\dot{x} = \frac{x_\infty(u) - x}{t_x(u)}\,, x \in \{h, n, s, c, q\}\,, u \in \{v_s, v_d, Ca\}$$

$$X(Ca) = min((Ca/250), 1)$$

The rate equations are calculated using the following equations:

$$x_\infty = \frac{\alpha_x}{\alpha_x + \beta_x}$$

$$\tau_x = \frac{1}{\alpha_x + \beta_x}$$

$$\alpha_m = \frac{0.32(-46.9 - v_s)}{exp((-46.9 - v_s)/4) - 1}$$

$$\beta_m = \frac{0.28(v_s + 19.9)}{exp((v_s + 19.9)/5) - 1}$$

$$\alpha_n = \frac{0.016(-24.9 - v_s)}{exp((-24.9 - v_s)/5) - 1}$$

$$\beta_n = 0.25\, exp\,(-1 - 0.025 v_s)$$

$$\alpha_h = 0.128\, exp\,((-43 v_s)/18)$$

$$\beta_h = \frac{4}{1 + exp((-20 - v_s)/5)}$$

$$\alpha_s = \frac{1.6}{1 + exp(-0.072(v_d - 5))}$$

$$\beta_s = \frac{0.02(v_d + 8.9)}{exp((v_d + 8.9)/5) - 1}$$

$$\alpha_c = \begin{cases} \frac{exp\left((v_d + 50)/11 - (-53.3 - v_d)/27\right)}{18.975}, & if\ v_d \le -10 \\ 2exp\left((-53.3 - v_d)/27\right), & if\ v_d > -10 \end{cases}$$

$$\beta_c = \begin{cases} 2exp\left((-53.3 - v_d)/27\right), & if\ v_d \le -10 \\ 0, & if\ v_d > -10 \end{cases}$$

$$\alpha_q = min(0.00002Ca, 0.01)$$

$$\beta_q = 0.001$$

Parameter values for pyramidal cell are:

Parameter	Value	Parameter	Value
v_L	-60mV	$g_{L,s} = g_{L,d}$	-0.1mS
v_{Na}	60mV	g_{Na}	30mS
v_{Ca}	80mV	g_{Ca}	10mS
v_K	-75mV	g_{K-DR}	15mS
g_c	2.1mS	g_{K-AHP}	0.8mS
C_m	3.0uF	g_{K-C}	15mS
p	0.5		

2. Interneuron Cell:

The interneuron cell is modelled using Wang & Buzsaki (1996) model. It has a single compartment with membrane potential v_i.

$$C_{m,i}\dot{v}_i = -I_{L,i} - I_{Na,i} - I_{K,i} - I_{syn,i} + I_i \quad (3)$$

Equation (3) explains the dynamics of the interneuron. $I_{L,i}$ is the leak current, $I_{Na,i}$ is the sodium current, and I_{Ki} is the delayed-rectifier potassium current. These currents are calculated as:

$$I_{L,i} = g_{L,i}\,(v_i - v_{L,i})$$

$$I_{Na,i} = g_{Na,i}\, m_{i,\infty}^3(v_i) h(v_i - v_{Na,i})$$

$$I_{K,i} = g_{K,i}\, n_i^4 (v_i - v_{K,i})$$

$$\dot{x} = \emptyset_x, (\alpha_x(1-x) - \beta_x x, \quad x \epsilon \{h_i, n_i\}$$

The kinetics of the gating variables are calculated using the following equations:

$$\alpha_{mi} = \frac{-0.1\,(v_i + 35)}{\exp\,(-0.1\,(v_i + 35)) - 1}$$

$$\beta_{mi} = 4\,exp\,(-(\,v_i + 60)/18)$$

$$\alpha_{ni} = \frac{-0.01\,(v_i + 34)}{\exp\,(-0.01\,(v_i + 34)) - 1}$$

$$\beta_{ni} = 0.125\,\exp\,(-(v_i + 44)/80)$$

$$\alpha_{hi} = 0.07\,\exp(-\,(v_i + 58)/20)$$

$$\beta_{hi} = \frac{1}{1+\exp\,(-0.1(v_i+28))}$$

Parameter values for interneuron cell are:

Parameter	Value	Parameter	Value
$v_{L,i}$	-65mV	$g_{L,i}$	-0.1mS
$v_{Na,i}$	55mV	$g_{Na,i}$	35mS
$v_{K,i}$	-75mV	$g_{K,i}$	9mS
$\emptyset_h$	5	$\emptyset_n$	1
$C_{m,i}$	1.0uF		

3. Synapses:

All synapses are modelled using the following equations:

$$I_{syn} = g_{syn} S_{syn} (v_{post} - v_{syn})$$

$$\dot{S}_{syn} = \alpha_{syn} (1 - s_{syn}) F(v_{pre}(t - \tau_d), \theta_{syn}, \alpha_{syn}) - \beta_{syn} s_{syn} \quad (4)$$

Equation (4) explains the dynamics of the synapses. F (x, θ, σ) is a sigmoid/softmax function, $F(x) = 1 / (1 + \exp(-(x - \theta)/\sigma)$, v_{pre} is the membrane potential of presynapse neuron and v_{post} is the membrane potential of postsynaptic neuron. Rise and decay rate of the synapse is,

$\alpha_{syn} = 1 / \tau_{rise}$ & $\beta_{syn} = 1 / \tau_{decay}$. τ_d is the synaptic delay time.

Parameter values for the synapses are:

Parameter	Value	Parameter	Value
$v_{syn,d,s}$	-65mV	$v_{syn,d,s}$	-80mV
$\alpha_{syn,d,s}$	1	$\theta_{syn,d,s}$	0mS
$\tau_{rise,fast}$	1ms	$\tau_{deacy,fast}$	9ms
$\tau_{rise,slow}$	5ms	$\tau_{decay,slow}$	20ms

4. Plots:

1. Verification of implementation of Pinksy and Rinzel Cell in Brian Simulator by providing various dendritic currents to confirm adherence of Pyramidal Cell's activity with bifurcation diagram

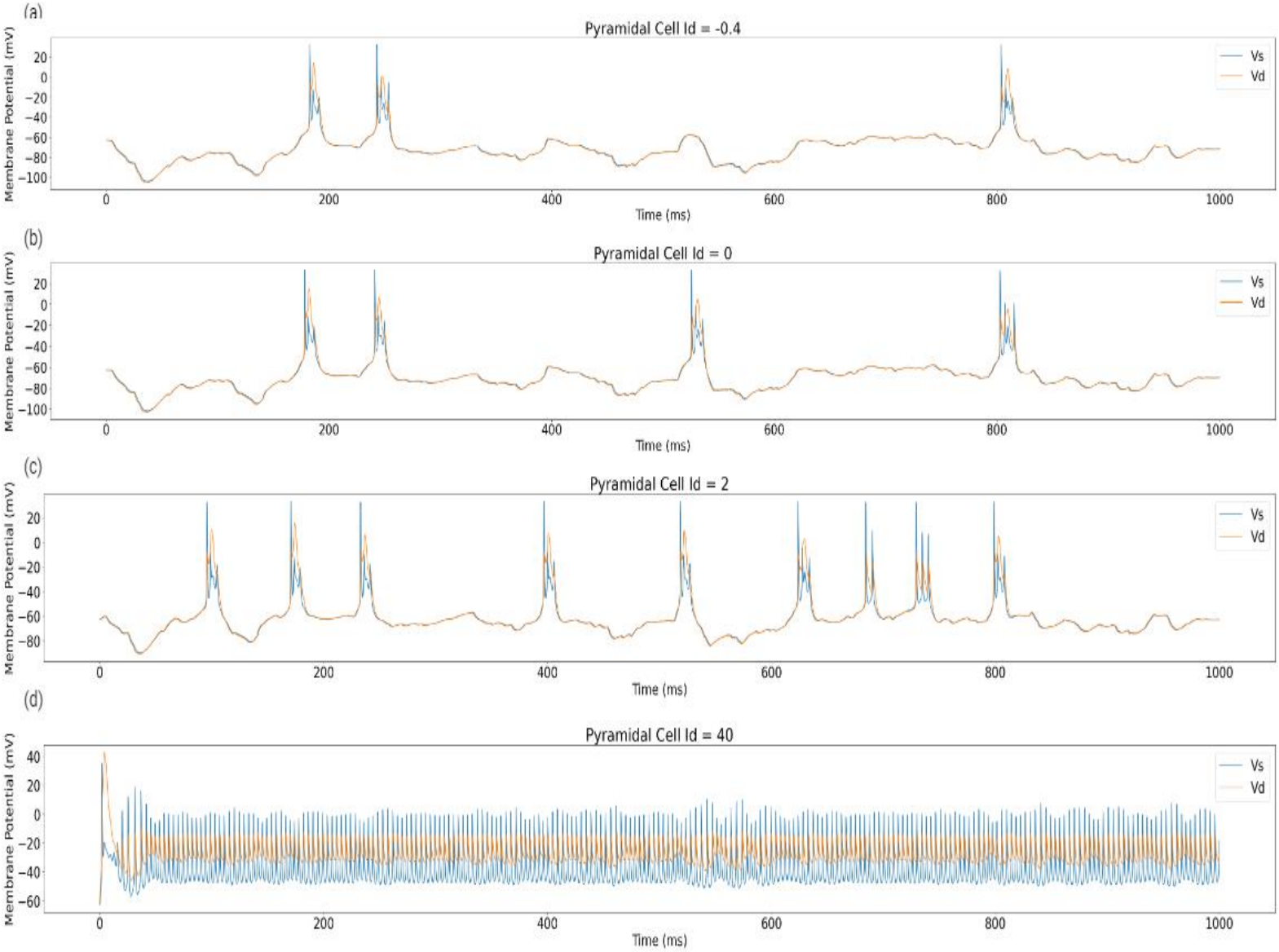

1. Cross-Correlation between pyramidal cell spike times and interneuron spike times for dendritic inhibition (left column) and somatic inhibition (right columns)

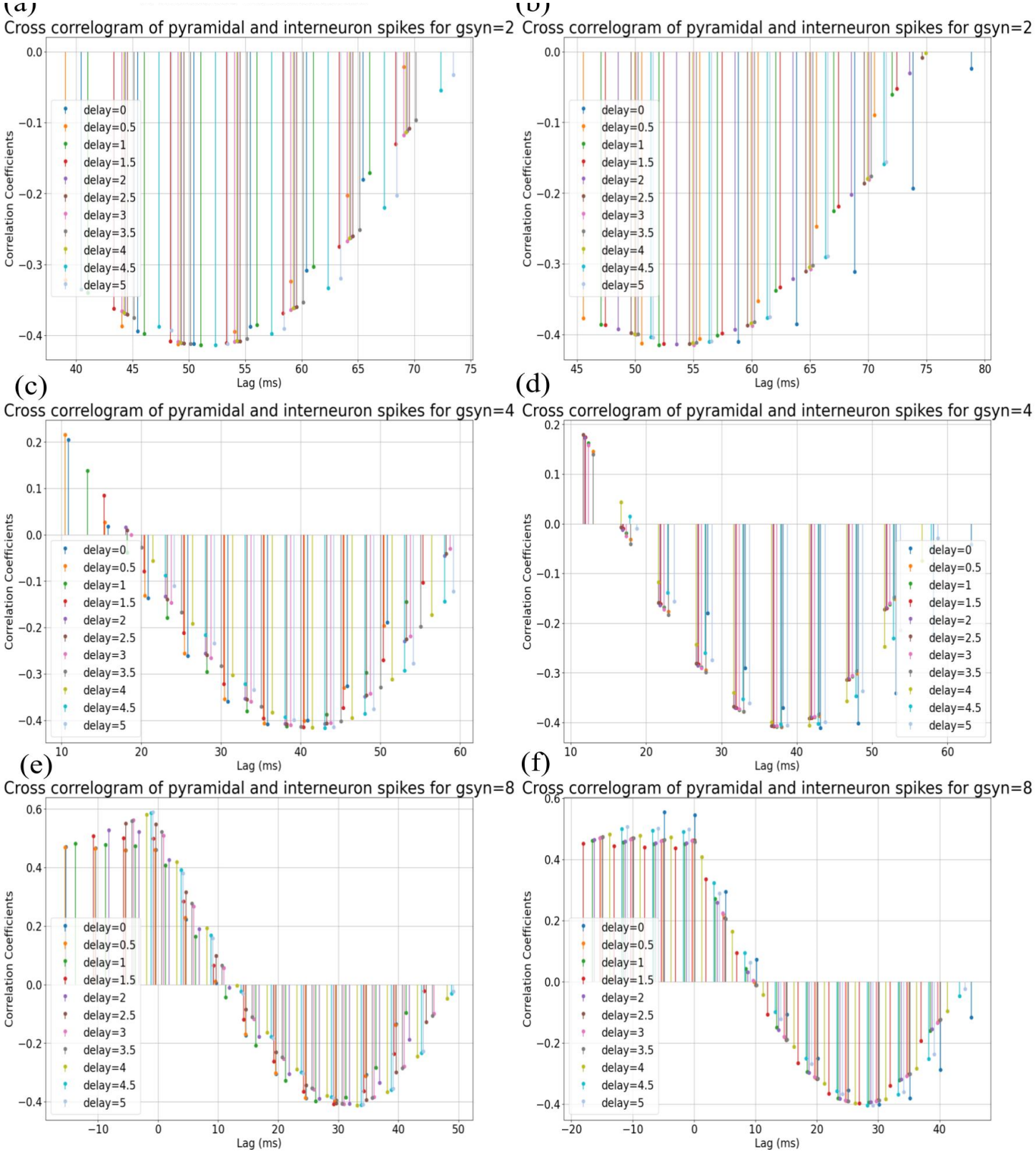

References:

Banks, M. I., Li, T.-B., & Pearce, R. A. (1998). The Synaptic Basis of GABA $_{A,slow}$. *The Journal of Neuroscience*, *18*(4), 1305–1317. https://doi.org/10.1523/JNEUROSCI.18-04-01305.1998

Banks, M. I., White, J. A., & Pearce, R. A. (2000). Interactions between Distinct GABAA Circuits in Hippocampus. *Neuron*, *25*(2), 449–457. https://doi.org/10.1016/S0896-6273(00)80907-1

Bartos, M., Vida, I., Frotscher, M., Meyer, A., Monyer, H., Geiger, J. R. P., & Jonas, P. (2002). Fast synaptic inhibition promotes synchronized gamma oscillations in hippocampal interneuron networks. *Proceedings of the National Academy of Sciences*, *99*(20), 13222–13227. https://doi.org/10.1073/pnas.192233099

Booth, V., & Bose, A. (2001a). Neural Mechanisms for Generating Rate and Temporal Codes in Model CA3 Pyramidal Cells. *Journal of Neurophysiology*, *85*(6), 2432–2445. https://doi.org/10.1152/jn.2001.85.6.2432

Booth, V., & Bose, A. (2001b). Regulating firing rate of networks of pyramidal cells. *Neurocomputing*, *38–40*, 497–504. https://doi.org/10.1016/S0925-2312(01)00380-0

Booth, V., & Bose, A. (2002). Burst synchrony patterns in hippocampal pyramidal cell model networks. *Network: Computation in Neural Systems*, *13*(2), 157–177. https://doi.org/10.1080/net.13.2.157.177

Bose, A., Booth, V., & Recce, M. (2000). A temporal mechanism for generating the phase precession of hippocampal place cells. *Journal of Computational Neuroscience*, *9*(1), 5–30. https://doi.org/10.1023/A:1008976210366

Dubey, M., Pascual-Garcia, M., Helmes, K., Wever, D. D., Hamada, M. S., Kushner, S. A., & Kole, M. H. (2022). Myelination synchronizes cortical oscillations by consolidating parvalbumin-mediated phasic inhibition. *eLife*, *11*, e73827. https://doi.org/10.7554/eLife.73827

Ewell, L. A., & Jones, M. V. (2010). Frequency-Tuned Distribution of Inhibition in the Dentate Gyrus. *The Journal of Neuroscience*, *30*(38), 12597–12607. https://doi.org/10.1523/JNEUROSCI.1854-10.2010

Ferrante, M., Migliore, M., & Ascoli, G. A. (2009). Feed-forward inhibition as a buffer of the neuronal input-output relation. *Proceedings of the National Academy of Sciences*, *106*(42), 18004–18009. https://doi.org/10.1073/pnas.0904784106

Gloveli, T., Dugladze, T., Rotstein, H. G., Traub, R. D., Monyer, H., Heinemann, U., Whittington, M. A., & Kopell, N. J. (2005). Orthogonal arrangement of rhythm-generating microcircuits in the hippocampus. *Proceedings of the National Academy of Sciences*, *102*(37), 13295–13300. https://doi.org/10.1073/pnas.0506259102

Gloveli, T., Dugladze, T., Saha, S., Monyer, H., Heinemann, U., Traub, R. D., Whittington, M. A., & Buhl, E. H. (2005). Differential involvement of oriens/pyramidale interneurones in hippocampal network oscillations *in vitro*. *The Journal of Physiology*, *562*(1), 131–147. https://doi.org/10.1113/jphysiol.2004.073007

Gonchar, Y. (1997). Three distinct families of GABAergic neurons in rat visual cortex. *Cerebral Cortex*, *7*(4), 347–358. https://doi.org/10.1093/cercor/7.4.347

Jonas, P., & Buzsaki, G. (2007). Neural inhibition. *Scholarpedia*, *2*(9), 3286. https://doi.org/10.4249/scholarpedia.3286

Kamondi, A., Acsády, L., Wang, X.-J., & Buzsáki, G. (1998). Theta oscillations in somata and dendrites of hippocampal pyramidal cells in vivo: Activity-dependent phase-precession of action potentials. *Hippocampus*, *8*(3), 244–261. https://doi.org/10.1002/(SICI)1098-1063(1998)8:3<244::AID-HIPO7>3.0.CO;2-J

Klausberger, T. (2009). GABAergic interneurons targeting dendrites of pyramidal cells in the CA1 area of the hippocampus. *European Journal of Neuroscience*, *30*(6), 947–957. https://doi.org/10.1111/j.1460-9568.2009.06913.x

Miles, R., Tóth, K., Gulyás, A. I., Hájos, N., & Freund, T. F. (1996). Differences between Somatic and Dendritic Inhibition in the Hippocampus. *Neuron*, *16*(4), 815–823. https://doi.org/10.1016/S0896-6273(00)80101-4

Mittmann, W., Chadderton, P., & Häusser, M. (2004). Neuronal Microcircuits: Frequency-Dependent Flow of Inhibition. *Current Biology*, *14*(19), R837–R839. https://doi.org/10.1016/j.cub.2004.09.036

Pearce, R. A. (1993). Physiological evidence for two distinct GABAA responses in rat hippocampus. *Neuron*, *10*(2), 189–200. https://doi.org/10.1016/0896-6273(93)90310-N

Pinsky, P. F., & Rinzel, J. (1994). Intrinsic and network rhythmogenesis in a reduced traub model for CA3 neurons. *Journal of Computational Neuroscience*, *1*(1–2), 39–60. https://doi.org/10.1007/BF00962717

Pouille, F., Marin-Burgin, A., Adesnik, H., Atallah, B. V., & Scanziani, M. (2009). Input normalization by global feedforward inhibition expands cortical dynamic range. *Nature Neuroscience*, *12*(12), 1577–1585. https://doi.org/10.1038/nn.2441

Pouille, F., & Scanziani, M. (2001). Enforcement of Temporal Fidelity in Pyramidal Cells by Somatic Feed-Forward Inhibition. *Science*, *293*(5532), 1159–1163. https://doi.org/10.1126/science.1060342

Stella, F., & Treves, A. (2011). Associative Memory Storage and Retrieval: Involvement of Theta Oscillations in Hippocampal Information Processing. *Neural Plasticity*, *2011*, 1–15. https://doi.org/10.1155/2011/683961

Tamás, G., Buhl, E. H., & Somogyi, P. (1997). Fast IPSPs elicited via multiple synaptic release sites by different types of GABAergic neurone in the cat visual cortex. *The Journal of Physiology*, *500*(3), 715–738. https://doi.org/10.1113/jphysiol.1997.sp022054

Tiesinga, P. H. E., Fellous, J., José, J. V., & Sejnowski, T. J. (2001). Computational model of carbachol-induced delta, theta, and gamma oscillations in the hippocampus. *Hippocampus*, *11*(3), 251–274. https://doi.org/10.1002/hipo.1041

Tort, A. B. L., Rotstein, H. G., Dugladze, T., Gloveli, T., & Kopell, N. J. (2007). On the formation of gamma-coherent cell assemblies by oriens lacunosum-moleculare interneurons in the hippocampus. *Proceedings of the National Academy of Sciences*, *104*(33), 13490–13495. https://doi.org/10.1073/pnas.0705708104

Traub, R. D., Wong, R. K., Miles, R., & Michelson, H. (1991). A model of a CA3 hippocampal pyramidal neuron incorporating voltage-clamp data on intrinsic conductances. *Journal of Neurophysiology*, *66*(2), 635–650. https://doi.org/10.1152/jn.1991.66.2.635

Virtanen, P., Gommers, R., Oliphant, T. E., Haberland, M., Reddy, T., Cournapeau, D., Burovski, E., Peterson, P., Weckesser, W., Bright, J., Van Der Walt, S. J., Brett, M., Wilson, J., Millman, K. J., Mayorov, N., Nelson, A. R. J., Jones, E., Kern, R., Larson, E., … Vázquez-Baeza, Y. (2020). SciPy 1.0: Fundamental algorithms for scientific computing in Python. *Nature Methods*, *17*(3), 261–272. https://doi.org/10.1038/s41592-019-0686-2

Wang, X.-J., & Buzsáki, G. (1996). Gamma Oscillation by Synaptic Inhibition in a Hippocampal Interneuronal Network Model. *The Journal of Neuroscience*, *16*(20), 6402–6413. https://doi.org/10.1523/JNEUROSCI.16-20-06402.1996

White, J. A., Banks, M. I., Pearce, R. A., & Kopell, N. J. (2000). Networks of interneurons with fast and slow γ-aminobutyric acid type A ($GABA_A$) kinetics provide substrate for mixed gamma-theta rhythm. *Proceedings of the National Academy of Sciences*, *97*(14), 8128–8133. https://doi.org/10.1073/pnas.100124097

Whittington, M. A., Traub, R. D., Kopell, N., Ermentrout, B., & Buhl, E. H. (2000). Inhibition-based rhythms: Experimental and mathematical observations on network dynamics. *International Journal of Psychophysiology*, *38*(3), 315–336. https://doi.org/10.1016/S0167-8760(00)00173-2

Wierenga, C. J., & Wadman, W. J. (2003). Functional relation between interneuron input and population activity in the rat hippocampal cornu ammonis 1 area. *Neuroscience*, *118*(4), 1129–1139. https://doi.org/10.1016/S0306-4522(03)00060-5

Wilson, H. R., & Cowan, J. D. (1973). A mathematical theory of the functional dynamics of cortical and thalamic nervous tissue. *Kybernetik*, *13*(2), 55–80. https://doi.org/10.1007/BF00288786

Zeldenrust, F., De Knecht, S., Wadman, W. J., Denève, S., & Gutkin, B. (2017). Estimating the Information Extracted by a Single Spiking Neuron from a Continuous Input Time Series. *Frontiers in Computational Neuroscience*, *11*, 49. https://doi.org/10.3389/fncom.2017.00049

Zeldenrust, F., & Wadman, W. J. (2009). Two forms of feedback inhibition determine the dynamical state of a small hippocampal network. *Neural Networks*, *22*(8), 1139–1158. https://doi.org/10.1016/j.neunet.2009.07.015

Zeldenrust, F., & Wadman, W. J. (2013). Modulation of spike and burst rate in a minimal neuronal circuit with feed-forward inhibition. *Neural Networks*, *40*, 1–17. https://doi.org/10.1016/j.neunet.2012.12.008